Effect of untreated and thermoactivated construction spoil on microstructure and properties of low-carbon foam concrete

Junhui Zhang [a], Yu Wang [a], Yuxiang Tang [a,*], Xufu Wang [a], Fan Gu [a], Jianzhuang Xiao [b,c], Jianxin Li [d], Mingzhong Zhang [e]

[a] School of Transportation, Changsha University of Science & Technology, Changsha 410114, China
[b] College of Civil Engineering, Tongji University, Shanghai 200092, China
[c] College of Civil Engineering and Architecture, Guangxi University, Nanning 530004, China
[d] School of Future Transportation, Guangzhou Maritime University, Guangdong 510725, China
[e] Department of Civil, Environmental and Geomatic Engineering, University College London, London WC1E 6BT, UK

ARTICLE INFO

Keywords:
Foam concrete
Construction spoil
Thermoactivated treatment
Macroscopic properties
Microstructures

ABSTRACT

This study proposes to develop low-carbon foam concrete by replacing cement with construction spoil (CS). The influences of CS content, thermoactivated treatment and particle size on the microstructure and macro-properties of foam concrete were systematically studied. Key parameters analyzed included the fluidity, rheology, setting time and defoaming rate of fresh slurry, as well as the pore structure, phase composition, compressive strength, drying shrinkage and water transport of hardened concrete. Furthermore, life cycle assessment and cost analysis were employed to quantify the carbon footprint and cost of the material. The results showed that using untreated CS resulted in reduced fluidity, prolonged setting time, increased yield stress and plastic viscosity, and increased defoaming rate of fresh mixture, as well decreased hydration products, and reduced interconnected pores and average pore size, which weakened the strength, shrinkage and transport performance of hardened concrete. The heat treatment of CS effectively enhanced the early stability of foam concrete with CS, decreased the pore size and increased the pore sphericity due to the generated metakaolin components. With further use of finer-grained heat-treated CS, the induced hydration products increased, the interconnected pores decreased, and the proportion of small-sized spherical pores increased. These microstructural refinements significantly enhanced various macroscopic properties of the material. The use of either untreated or thermal-activated CS reduced the carbon emission and cost of foam concrete by up to about 28.2 % and 13.2 %, respectively.

1. Introduction

Foam concrete, as a lightweight construction material, exhibits adjustable density and strength, convenient production processes, excellent thermal insulation properties, and remarkable durability [1]. It is widely employed in transport infrastructure projects, such as soft ground treatment, reconstruction and expansion of roads, insulating roadbeds in permafrost regions and back filling of abutment [2]. Meanwhile, cement, as the main raw material for cement-based foam concrete, has a significant contribution to greenhouse gas emissions, accounting for around 8 % of total anthropogenic CO_2 emissions [3]. Under the goal of carbon neutrality and peaking, there is an urgent need to promote the low-carbon preparation of foam concrete.

For this purpose, one approach is to adopt carbon dioxide capture, utilization, and storage (CCUS) technology, while another is to seek alternatives to cement. Regarding the former, waste CO_2 can be converted into CO_2-aqueous foams to produce foam concrete [4,5], realizing the dual benefits of environmental protection and enhanced material performance [6,7]. Besides, construction solid waste (CSW) is often recycled and employed as a substitute for cement, reducing the carbon emissions of cement-based materials and achieving high-value utilization of solid waste [8,9]. Recently, many efforts have been made to clarify the impact of CSW on the performance of foam concrete. Aliabdo et al. [10] demonstrated that crushed clay brick powder enhanced the compressive strength of autoclaved aerated concrete, while it weakens the pore structures. Dang et al. [11] prepared alkali-activated foam concrete using recycled brick and concrete powder, and proved that this material had good insulation properties and mechanical strength.

* Corresponding author.
E-mail address: yxtang@csust.edu.cn (Y. Tang).

Pasupathy et al. [12] revealed that increasing the Na_2O concentration could significantly improve brick powder activity and optimized slurry coagulation characteristics and pore structures. The utilization of CSW to prepare green and low-carbon foam concrete has good feasibility, but usually has a significant impact on the microstructures and engineering properties of the material, which needs to be explored deeply and systematically.

Construction spoil (CS) is a type of CSW generated during civil engineering activities. Despite the large production and stock of CS, its resource utilization is relatively low [13]. One of the most effective ways to scale up CS consumption is to recycle it as a new construction and building material. Unfortunately, CS contains a high percentage of inactive components, such as quartz and feldspar, that is highly absorbent and does not participate in the hydration reaction [14]. Thus, untreated CS serves only as a pore-filling material and lacks inherent activity, causing the clay minerals in it that adversely affect the hydration products and reduce the fluidity and mechanical properties of the material.

To enhance the resource utilization rate of CS and the added value of the prepared products, modification pretreatment methods are commonly employed to activate its potential activity and to mitigate its adverse effects on the preparation of building material. Typically, modification methods for CS include alkaline activation [15], mechanical grinding [16], and thermal activation treatment [17]. Studies have shown that materials prepared by alkali-activated CS exhibit excellent durability and effectively solidify heavy metals and toxic substances [18, 19]. Additionally, the alkali-activation process requires precise control of the concentration and content of activator, which carries the risk of alkali leaching and introduces extra environmental costs for subsequent disposal of the spent alkali solution [20]. In contrast, thermal-activated CS not only serves as a micro-aggregate filler, but also converts kaolin components into metakaolin and amorphous substances that exhibits pozzolanic activity [21]. Particularly in the southeastern coastal regions of China, construction waste predominantly consists of residual granite soil with high kaolinite content [22]. Moreover, given the widespread distribution of soft soil foundations in this area, it presents favorable prospects for the application of foam concrete. The mortar with heat-treated CS demonstrated better microstructures, enhanced strength, and improved resistance to chloride salt erosion [23]. The particle size of solid particles significantly influences the properties of cementitious materials, particularly in lightweight foam concrete systems. Generally, variations in solid particle size cause corresponding changes in surface roughness and grain mass, thereby affecting the workability of fresh paste and the early-stage stability of foam [24]. These factors ultimately have a significant impact on the microstructural evolution and macroscopic properties of hardened foam concrete [25]. Thus, the influence of thermoactivated treatment and particle size of CS on the properties of foam concrete with lightweight porous structures remains to be thoroughly investigated.

Therefore, this study aims to investigate the effects of CS contents, thermal treatment and particle size, on the various properties of prepared foam concrete, as presented in Fig. 1. These included the characteristics of the fresh slurry, such as fluidity, rheology, setting time and defoaming rate, as well as the microstructural and macroscopic properties after hardening. Specifically, the hardened microstructures comprised chemical composition, micro morphology and pore structures, and the macro-properties included mechanical strength, drying shrinkage behavior, water absorption. In addition, the life cycle assessment and cost analysis were employed to quantify the carbon footprint and cost of foam concrete for a comprehensive evaluation. Finally, the influence mechanism of CS type and dosage was revealed by combining macro-properties and microstructures.

2. Materials and methods

2.1. Raw materials and properties

The CS employed in this study was sourced from a foundation pit at a construction site in Guangzhou, China, which is a representative coastal metropolis characterized by widespread soft soil distribution, rapid urban renewal, and consequently massive CS generation. Given the higher kaolinite content observed within the 0–5.7 m depth range underground (i.e., areas exhibiting greater weathering) [26], CS was collected from this zone in this study. If the sampling depth exceeds 5 m, it is recommended to treat the samples using the water-washing method, which can effectively increase the content of kaolinite in CS [27].

As depicted in Fig. 1, considering that the main active components in CS are mostly distributed in fine particles, the soil was first crushed by a crusher, and then the collected waste CS was screened with a 1 mm sieve, which was named as untreated construction spoil (UCS). The oxide composition of UCS was determined by X-ray fluorescence (XRF) spectroscopy (see Table 1), and the results showed high proportions of

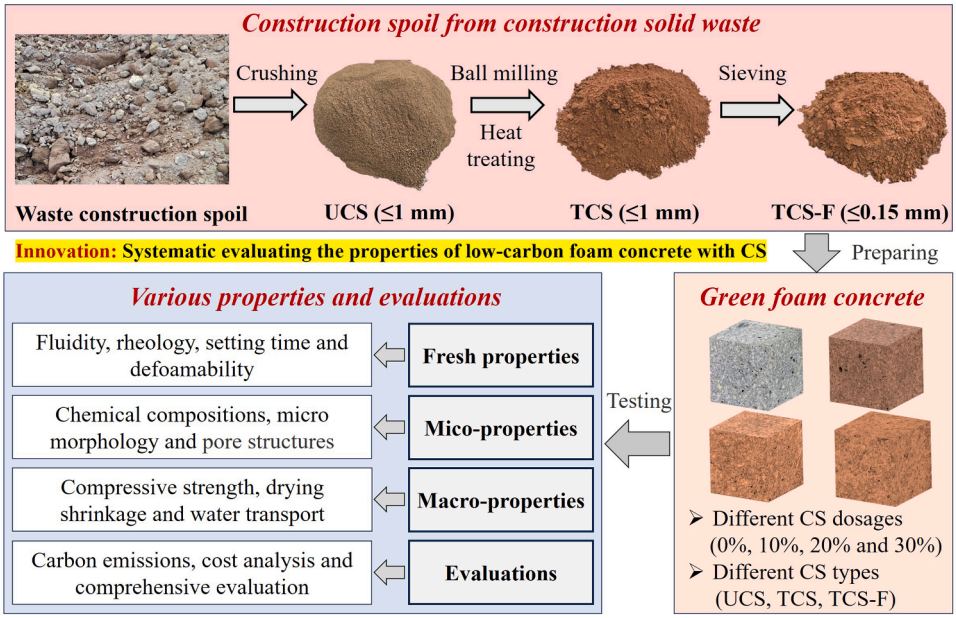

Fig. 1. Testing flow.

Table 1
Oxide chemistry of construction spoil and cement using XRF analysis (wt%).

Chemical compositions	SiO_2	Al_2O_3	Fe_2O_3	CaO	K_2O	SO_3	L.O.I
Construction spoil	55.01	29.95	10.25	0.07	2.26	0.13	2.33
Cement	22.02	6.19	2.65	58.99	0.58	2.67	6.9

SiO_2 (55.01 %) and Al_2O_3 (29.95 %), indicating that the kaolinite is the primary mineral phase. Its basic properties were tested according to the standard [28], with the results presented in Table 2. The liquid limit, plastic limit and plasticity index of CS were 40.8 %, 23.3 % and 17.5 , respectively, and it should be classified as a silty clay.

To determine the optimal temperature of thermal activation, thermogravimetric (TG) tests were conducted on the CS treated at 700°C, 800°C, and 900°C, with the results presented in Fig. 2. It can be observed that significant weight loss still occurs at 700°C, indicating that kaolinite has not been fully activated at this temperature. As the temperature rises to 800°C, the dihydroxylation reaction is more thorough. While at 900°C, the residual mass loss shows no significant change compared to 800°C. This demonstrates that the thermal activation reaction of kaolinite approaches completion at 800°C. Similar findings have been reported in studies by Hu et al. [17] and Li et al. [27]. Therefore, the optimal activation temperature for CS was determined to be 800°C in this study.

The kaolinite content in the CS used was calculated to be approximately 52.27 % from Eq. (1), which is within the mid-range of the local CS (23.8 %-69.2 %) [22]. Besides, existing study [29] have clearly proposed that a content of 40 % of kaolinite is proposed as minimum threshold value to qualify kaolinitic clays as suitable for use as mineral admixtures after calcination. For CS containing low levels of kaolinite, thermal activation treatment may not be advisable. Therefore, the CS utilized in this study is representative of CS used as a cement substitute after calcination in this region.

$$Mineral\ content = (M_1 - M_2)/M \times M_k/M_w \quad (1)$$

where M_1=Mass at lower dehydroxylation temperature; M_2=Mass at upper dehydroxylation temperature; M=Mass of sample at 200°C; Mk=Molecular mass of kaolinite; Mw = Molecular mass of water.

To enhance the pozzolanic reactivity, UCS was ground and thermal treated to produce treated construction spoil (TCS). Specifically, UCS was first ball-milled for 18 min, then heated in an SX2–5–12A muffle furnace at a heating rate of 15 °C/min to 800°C and subjected to a 2 h isothermal holding period to ensure homogeneous activation, followed by controlled cooling to room temperature. As per the fact that finer particles exhibit higher cementitious activity [30], the TCS was sieved through a 0.15 mm mesh to obtain TCS with finer particles (denoted as TCS-F).

Fig. 3 illustrates the appearances and particle size distributions of cement, UCS, TCS, and TCS-F. A clear color variation could be observed, i.e., gray for cement, light yellow for USC, and reddish-brown for TCS/TCS-F. Besides, the median particle sizes (D_{50}) of cement, UCS, TCS, and TCS-F were 17.65 μm, 92.43 μm, 45.10 μm, and 15.42 μm, respectively. Compared with cement, the particle size of CS was larger, while that of TCS remained larger despite being sieved, which may be attributed to the agglomeration phenomenon due to the adhesion of fine particles during thermal activation of CS [31]. It is obvious that TCS-F exhibited a

Table 2
The basic characteristics of construction spoil.

Natural moisture content (%)	Liquid limit (%)	Plastic limit (%)	Plasticity index	Free swelling ratio (%)	Organic matter content (g/kg)	pH
18	40.8	23.3	17.5	30	2.86	6.70

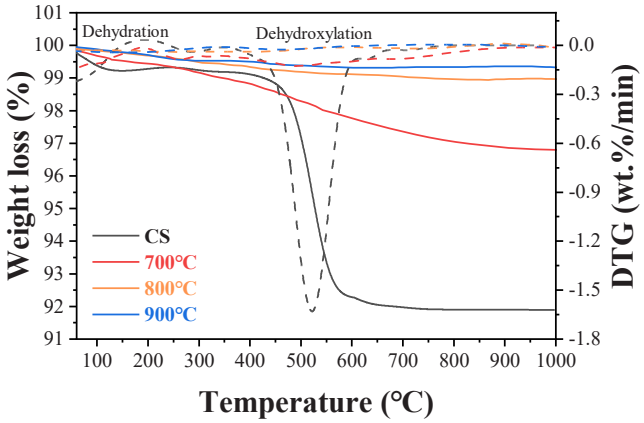

Fig. 2. TG results of CS under different thermal activation temperatures.

finer particle size, similar to that of cement, facilitating its pozzolanic activity and filling effect in cementitious materials.

Fig. 4 presents the chemical composition and micro-morphology of cement, UCS, TCS, and TCS-F by using scanning electron microscopy (SEM), XRD, and FTIR. As seen from the SEM images, the UCS particles showed an irregular granular structure with pseudo-hexagonal platy layered kaolinite, which was compact, low porosity and structurally disordered [32]. Both the particles of TCS and TCS-F retained the pseudo-hexagonal platy layered morphology, indicating that the particle shape of CS remained unchanged after thermal activation.

From the XRD analysis, it can be seen that the UCS contained a lot of SiO_2, which is inert and rarely participated in hydration reactions. Kaolinite was basically undetectable at 12.4° in the XRD pattern of TCS, indicating a significant reduction in crystallinity, which can be attributed to the decomposition of kaolinite into reactive metakaolin upon heating. Besides, the intensity of SiO_2 was reduced after heat treatment, which might lead to the generation of more active amorphous components in TCS. As per the FTIR analysis results, it can be found that, after thermal treatment (i.e., TCS), the three absorption bands of OH (3600–3700 cm^{-1}) and the peak of Al-OH bands (910 cm^{-1}) disappeared, indicating that thermal treatment caused significant destruction of the crystal structure of CS. Additionally, a notable shift in the Si-O-Si stretching vibration peak at 794 cm^{-1} was observed, which is consistent with the previous XRD results. It is noted that TCS and TCS-F only differ in particle size, so their XRD and FTIR results are similar.

2.2. Mix proportions

In this study, ten types of foam concretes with various CS type and content were designed. The CS used were UCS, TCS, and TCS-F at 0 %, 10 %, 20 %, and 30 % by weight of cement. Table 3 lists the specific mix proportions. The water-to-binder ratio was set at 0.425. A naphthalene-based superplasticizer was used at a content of 3 wt.‰. A composite reinforcing foaming agent was selected as the foaming agent, and hydroxypropyl methylcellulose (HPMC) was used as the foam stabilizer. The foaming agent, foam stabilizer, and aqueous solution were thoroughly mixed at a ratio of 1:0.02:30, after which the mixture was poured into a foaming machine to produce foam with a density of approximately 50 kg/m^3, ensuring the homogeneity and stability of the foam.

During the experiment, the wet and dry densities of foam concrete in each group were determined and the results are listed in Table 3. The results showed that the densities of foam concrete with different mix ratios are well consistent, with the wet density ranging from 798.5 to 829.7 kg/m^3 and the dry density ranging from 675.8 to 729.0 kg/m^3 . Among them, the maximum difference in density is less than 100 kg/m^3 . As per the relevant provisions of JGJ/T 341–2014 [33], it can be determined that the foamed concrete in all test groups is at the same

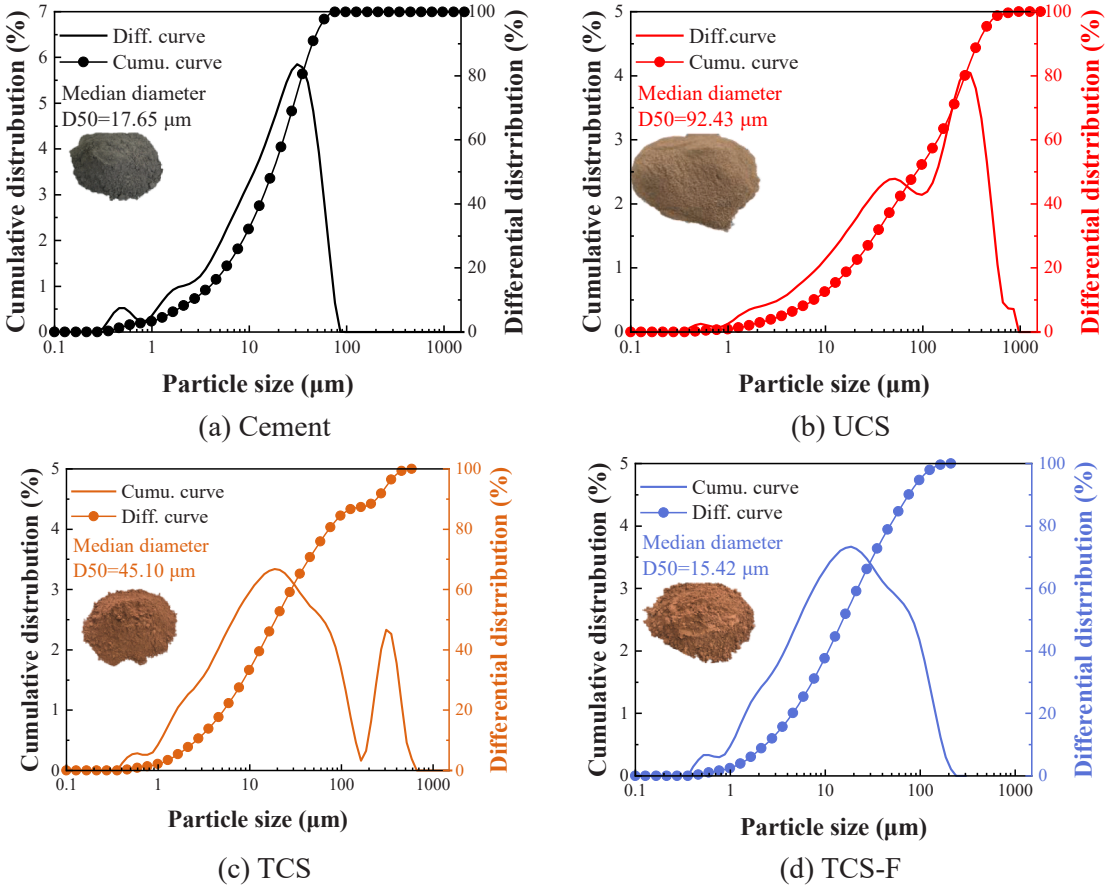

Fig. 3. Appearances and particle size distributions of un-treated and thermoactivated CS.

density grade. Thus, the effect of density on the properties of foam concrete can be considered negligible.

2.3. Sample preparation and test methods

Cement and CS were mixed in a mixer for 2 min, followed by the addition of water and continuous stirring for 3 min to obtain a slurry with good fluidity. Finally, the preformed foam was mixed with the slurry and stirred for 3 min to form a homogeneous fresh foam concrete. Part of the prepared fresh mixture was used to test its fluidity, rheology, setting times and defoaming rate, while the other part was poured into steel molds with dimensions of $40 \times 40 \times 40$ mm^3 and $40 \times 40 \times 160$ mm^3, which were then covered with plastic film to prevent moisture loss. After 48 h, the hardened specimens were demolded and cured under 20 ± 2°C and 95 ± 2 % relative humidity until the testing age. Fig. 1 presents the experimental testing and evaluation framework of this study. The foam concretes with different contents of UCS, TCS, and TCS-F were prepared to characterize their macroscopic properties and microstructures in both fresh and hardened states.

2.3.1. Fresh properties of foam concrete

The properties of fresh foam concrete encompassed fluidity, rheology, setting times, and defoaming rate. For fluidity, a micro-slump tester with both height and diameter of 80 mm was used to measure the flowability of the fresh mixture and its time-dependent loss. Specifically, the variation in flow diameters was measured with a ruler at 0, 30, 60, and 90 min to assess the loss. The rheological properties were determined using a TR-MPI rheometer. During the test, the shear rate was gradually increased to 60 s^{-1} in 8 sequential steps to measure the dynamic yield stress and plastic viscosity of the paste after 5 min of standing, the shear rate was gradually decreased from 60 s^{-1} to 0 s^{-1} within 160 s, and 8 sets of data were recorded during this process [34]. In addition, the Bingham model was adopted to calculate the rheological parameters of the fresh foam concrete, and the model expression was as follows:

$$\tau = \tau_0 + \mu\gamma \tag{2}$$

where τ, τ_0, μ, and γ are the fitting and calculation results of shear stress, yield stress, plastic viscosity, and shear rate, respectively.

The initial and final setting times were determined according to standard JGJ/T 341–2014 [33] using a Vickers meter. The defoaming rate was evaluated according to standard TJG F1001–2011 [35]. In detail, after preformed foam was mixed with the cement paste in a mixing pot for 3 min, the mixture was sampled with a 1 L cylinder and weighed. This process was repeated six times and the results were calculated as follows:

$$\delta = \frac{\rho_{max} - \rho_0}{\rho_0} \tag{3}$$

where δ, ρ_0 and ρ_{max} are the defoaming rate, initial density and maximum density, respectively.

2.3.2. Microstructure characterization

The properties of hardened foam concrete included microstructures, compressive strength, drying shrinkage, and transport properties. Among these, the microstructures were characterized by the chemical composition, micro-morphology, and pore structures of typical samples. For chemical composition measurement, specimens were ground into powder and sieved to a particle size below 0.075 mm. The powdered samples were employed to analyze the chemical components and

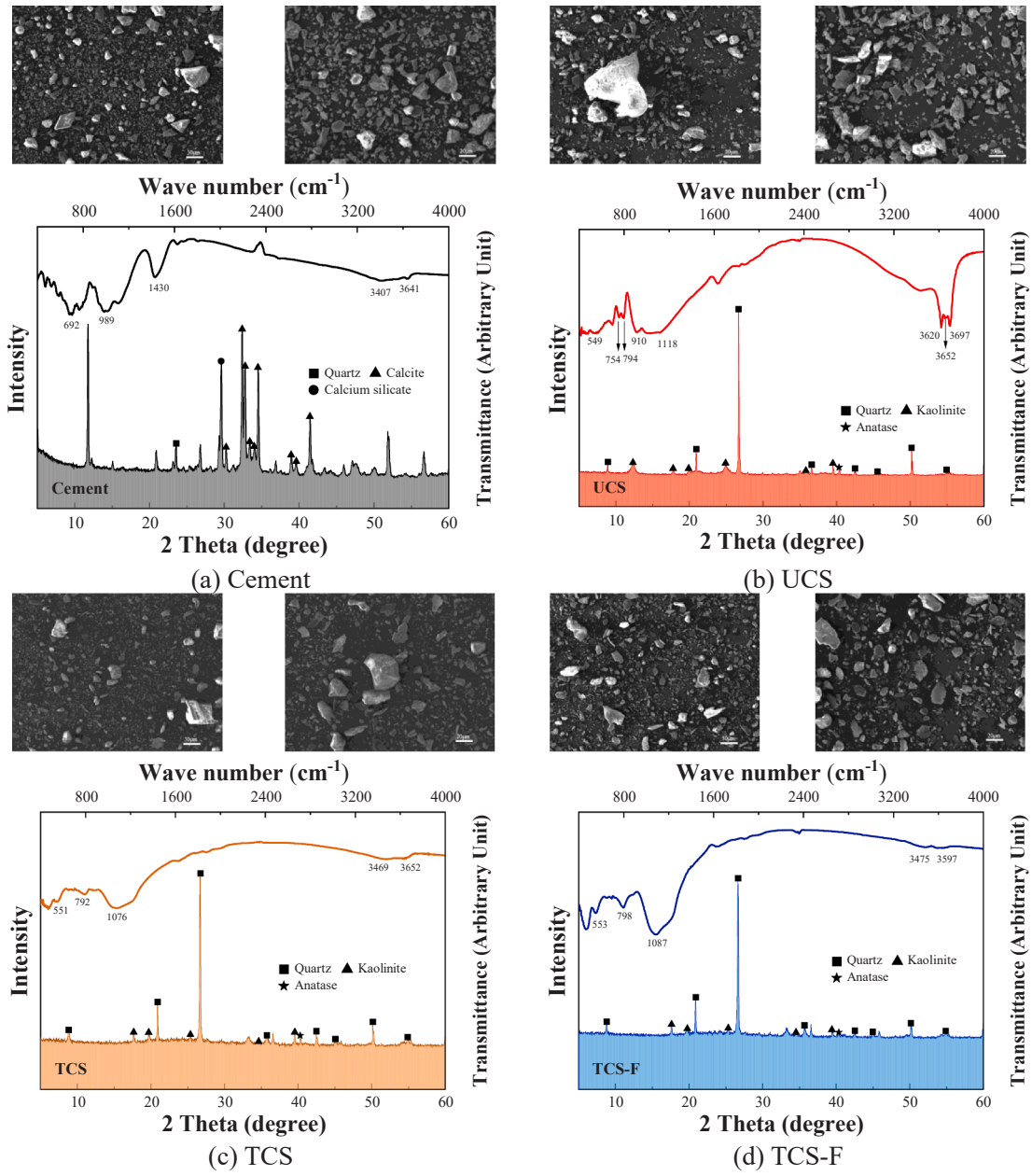

Fig. 4. SEM image, XRD pattern and FTIR spectroscopy of un-treated and thermoactivated CS.

Table 3
Mix ratios of foam concrete (kg).

Samples	Cement	CS	TCS	TCS-F	Water	Foam	Wet density (kg/m^3)	Dry density (kg/m^3)
Ref.	1000	0	0	0	425	70	807.7	684.0
10UCS	900	100	0	0	425	70	822.6	690.9
20UCS	800	200	0	0	425	70	829.7	687.3
30UCS	700	300	0	0	425	70	815.7	675.8
10TCS	900	0	100	0	425	70	798.5	701.7
20TCS	800	0	200	0	425	70	822.4	720.6
30TCS	700	0	300	0	425	70	812.5	714.4
10TCS-F	900	0	0	100	425	70	818.7	717.4
20TCS-F	800	0	0	200	425	70	827.7	728.0
30TCS-F	700	0	0	300	425	70	814.9	706.4

Notes: Specimen Ref. was defined as the referenced foam concrete without CS, while Specimen AB was denoted as the foam concrete with Type B CS at A% content

crystalline phase composition by using thermogravimetry (TG), X-ray diffraction (XRD), and Fourier transform infrared spectroscopy (FTIR). After 28-days of curing, foam concrete was sliced, and the internal pore structures of the core was observed using an optical microscope. The pore structures were further characterized by scanning electron microscopy (SEM) and then the pore size distribution was quantified using

commercial Image-Pro Plus software.

2.3.3. Macro-properties of hardened foam concrete

A series of experiments were conducted to determine the macroscopic properties of the materials, which comprised compressive strength, drying shrinkage, moisture absorption and thermal transmission. As per Chinese standards JG/T 266–2011 [36]and CJJ/T 177–2012 [37], the compressive strength of 40 mm cubes were tested at 7 days, 28-days, and 28-days under saturated water conditions, with a loading rate of 1 kN/s. For the drying shrinkage properties, as specified in GB/T 11969–2020 [38], specimens were demolded and immersed in water (20 ± 3°C) for 72 h, followed by placement in an environment of 20 ± 2°C and 45 ± 5 % relative humidity. A comparator was used to measure the initial length and post-shrinkage length of specimens during the 28-day test period. The drying shrinkage strain S of foam concrete was calculated using Eq. (4), where L_0 (mm) and L (mm) denote the initial and test lengths of the specimen.

$$S = \frac{(L_0 - L) \times 100}{L_0} \tag{4}$$

Water absorption is a common method for evaluating the transport properties and durability of cementitious materials. Cubic specimens with dimensions of 40 mm were used for the water absorption test [30]. The specimens were first placed in an air-drying oven set at 40°C for 72 h. Next, with the exception of two opposing side faces, other four sides of the specimens were sealed with a waterproof coating, and then they were immersed in water to allow unidirectional water penetration into the foam concrete. The equations for calculating the water absorption mass ΔW (g/m^2) and water absorption coefficient A_w (g/(m^{2}h$^{1/2}$)) of foam concrete are provided in Eqs. (5) and (6), where m_0 and m_1 denote the dry and absorbed water weights (g), S and t represent the contact area with water (m^2) and absorption duration (h), respectively.

$$\Delta W = \frac{(m_1 - m_0)}{S} \tag{5}$$

$$\Delta W = A_W\sqrt{t} \tag{6}$$

Neglecting the effect of gravity, the moisture transport can be further described by Eqs. (7) and (8), where a and b are the fitting coefficients, $A(t)$ represents the time-dependent capillary absorption coefficient (g/(m^{2}h$^{1/2}$)), and A_i =a × b denotes the time-dependent absorption rate (g/(m^{2}h$^{1/2}$)).

$$\Delta W = a[1 - \exp(-b\sqrt{t})] \tag{7}$$

$$A(t) = \frac{d\Delta W}{d\sqrt{t}} = A_i\exp(-b\sqrt{t}) \tag{8}$$

The water ingress of cementitious materials is closely associated with their porosity. The total porosity P of foam concrete was determined using the vacuum saturation experiment. The detailed calculation formula is provided in Eq. (9), where W_{dry} represents the weight of the fully-dried specimen, W_{sat} and W_{wat} are the weights of the saturated specimen in air and in water, respectively.

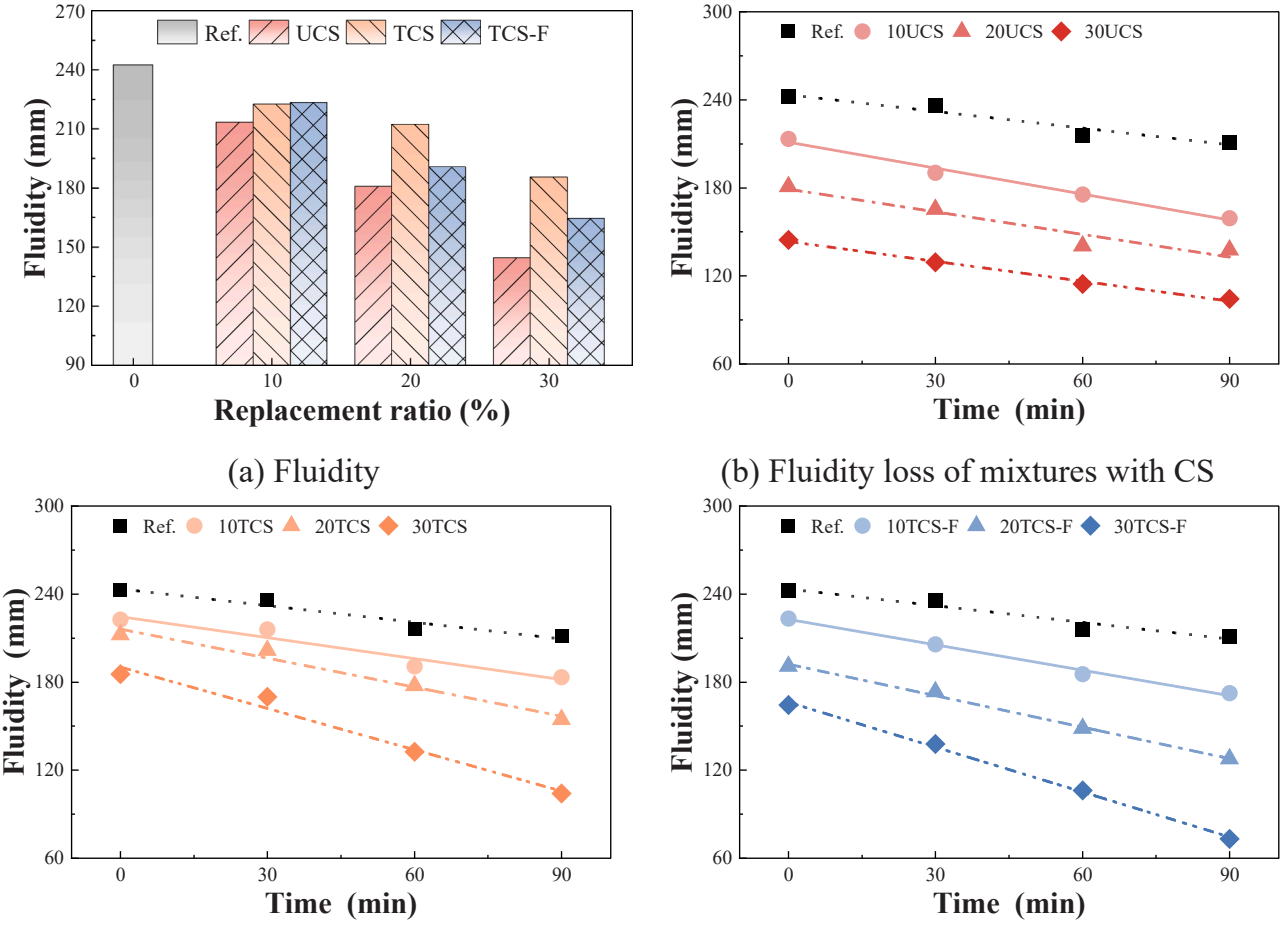

(a) Fluidity

(b) Fluidity loss of mixtures with CS

(c) Fluidity loss of mixtures with TCS

(d) Fluidity loss of mixtures with TCS-F

Fig. 5. Fluidity and time-dependent loss of fresh foam concrete.

$$P = \frac{(W_{sat} - W_{dry})}{(W_{sat} - W_{wat})} \times 100 \quad (9)$$

3. Experimental results

3.1. Properties of fresh foam concrete

3.1.1. Fluidity

The fluidity of fresh mixtures is a critical indicator of the workability of foam concrete. Fig. 5 presents the flowability and its time-dependent loss of all fresh foam concrete mixtures. As shown in Fig. 5(a), the initial fluidity of fresh mixtures decreased with increasing CS content. It can be seen from Fig. 5(b) and (c) that the foam concrete using TCS exhibited greater initial fluidity as compared to the foam concrete using UCS at the same dosage level. Except for the 10 % dosage, the inhibitory effect on the initial fluidity of foam concrete was more pronounced for TCS-F with smaller particle size. As depicted in Fig. 5(a–d), the fluidity of fresh slurry exhibited a significant time-dependent decline. It can be found that the trends in fresh mix fluidity over time were similar across UCS substitution rates (see Fig. 5(b)). By contrast, as shown in Fig. 5(c) and (d), increasing TCS dosage or decreasing particle size enhanced the time-dependent decline in slurry flowability. This is because, for TCS, in addition to the water absorption exhibited by porous particles like UCS, the active particles also consume water through their pozzolanic effect. This dual water consumption reduces the free water content within the system, increases the slip resistance between particles, and ultimately leads to a decrease in slurry fluidity [39].

3.1.2. Rheology

Fig. 6 shows the rheological results of all fresh foam concrete. The dynamic yield stress and plastic viscosity data were calculated based on the Bingham model, with the R^2 value of all fitting curves greater than 0.9. It can be seen that the yield stress and plastic viscosity of foam concrete increased with the CS dosage increasing from 10 % to 30 %. That indicates that the higher the CS dosage, the stronger the flow resistance and internal frictional resistance of the material. At a given CS dosage, the yield stress of foam concrete using TCS was reduced compared to UCS. In this case, the paste becomes more readily able to overcome resistance and flow, resulting in increased flowability (see Fig. 5(a)). In contrast to TCS group, the dynamic yield stress and plastic viscosity of the fine-grained TCS-F group increased by 27 %-193.6 % and 103 %-145.5 % respectively, (see Fig. 6(c)). This phenomenon occurs because the calcined clay finer possesses high surface area, strong negative surface charge, and layered particle structure, which collectively enhance the elevation of flocculation [40,41].

3.1.3. Setting times

Fig. 7 presents the initial and final setting times of all foam concrete mixtures. With the increase of UCS content, the initial and final setting times of foam concrete were gradually prolonged by about 14.4 %–34.9 % and 5.5 %–21.2 %, respectively. In contrast, the use of TCS resulted in shorter setting times. Higher TCS contents or finer particles further reduced the setting times, particularly due to variations in content. For example, the initial and final setting times of Specimens 10TCS, 20TCS, and 30TCS were reduced by 12.4 %–18.3 % and 7.9 %–24 %, respectively. While for Group TCS-F, they were decreased by 16.7 %–

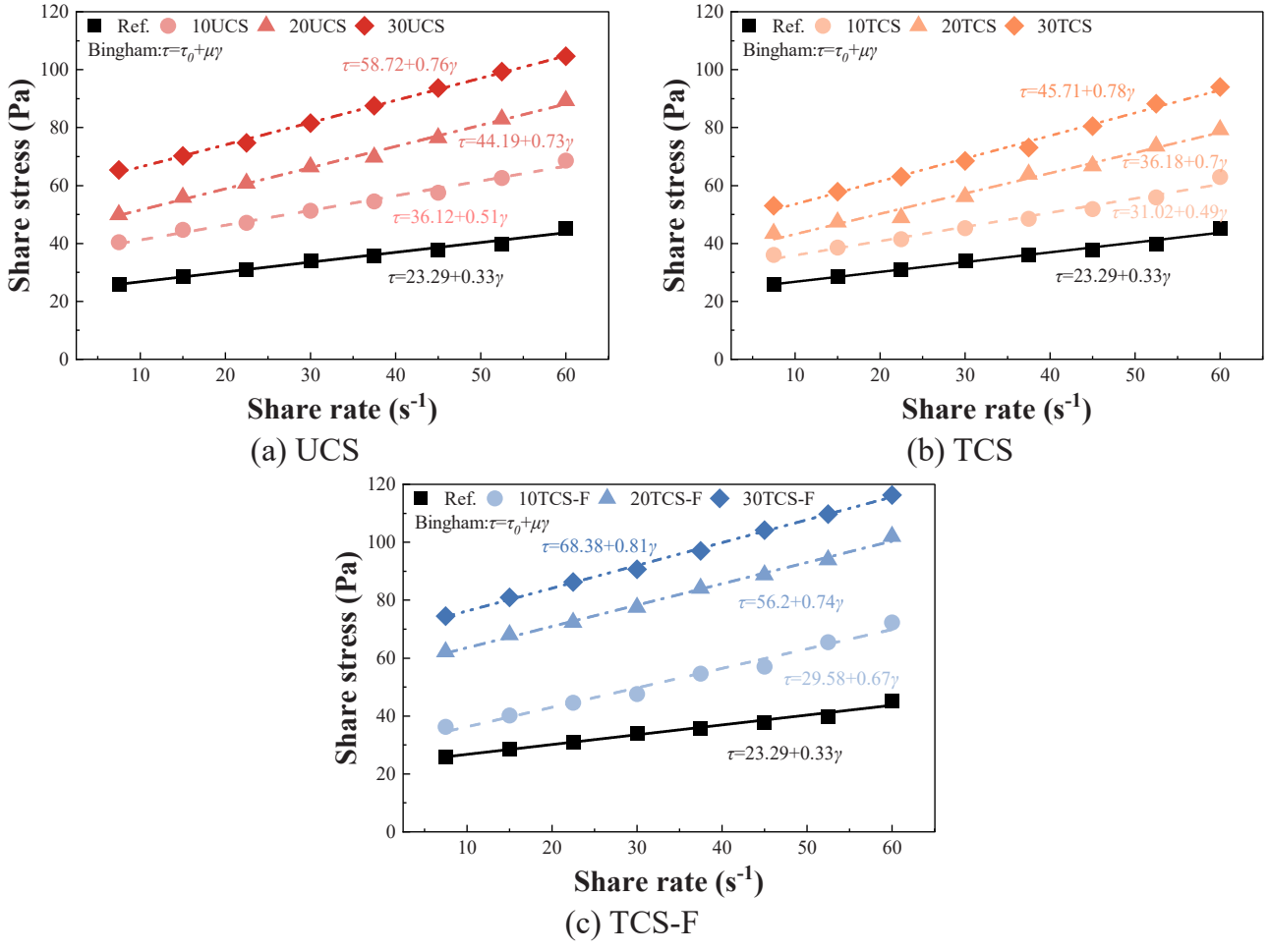

Fig. 6. Rheological Properties of fresh foam concrete.

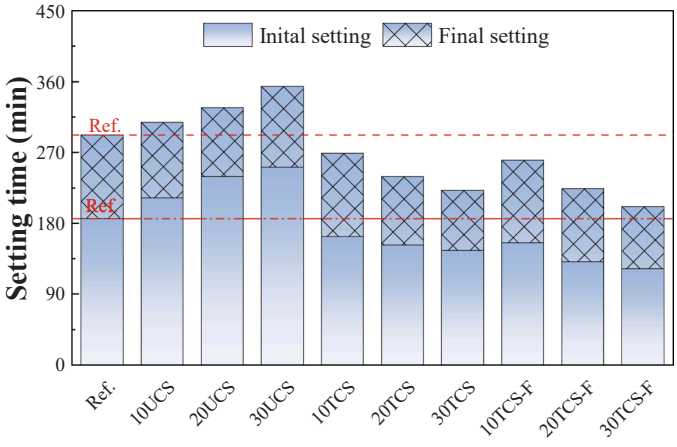

Fig. 7. Initial and final setting times of foam concrete.

49 % and 11 %–31.2 %, respectively.

3.1.4. Defoaming rate

Fig. 8 shows the defoaming rates of all foam concrete mixtures. It can be observed that, the defoaming rate of the mixtures gradually increased as the UCS content increased from 0 % to 30 %, up to about 44.5 %. With the increase of TCS content from 10 % to 30 %, the defoaming rate of the mixture decreased by approximately 23.9 %-34.4 %, which may be related to the shortening effect of TCS on the setting time of foam concrete (see Fig. 7). Furthermore, the defoaming rate of the mixture with TCS-F decreased by approximately 14.4 %-36.7 %, indicating that it is more significant in improving the foam stability of foam concrete.

3.2. Properties of hardened foam concrete

3.2.1. Chemical compositions

Taking the 20 % replacement rate as an example, the chemical compositions of foam concrete with different types of CS were conducted using DTG and XRD experiment, with results are presented in Fig. 9(a) and Fig. 9(b). As shown in Fig. 9(a), the DTG results exhibited four main characteristic peaks. The first peak, the sharpest one, occurred in the temperature range of about 100°C and represented the dehydration of the C-(A)-S-H gel and ettringite. It can be observed that this peak gradually intensified with the incorporation of TCS and TCS-F, indicating that thermal treatment and particle size reduction increased the hydration products in foam concrete with CS, including C-(A)-S-H and ettringite. The weak peak at 120–200°C reflected to the chemical weight loss of AFm, while the third and fourth peaks at about 450°C and 700°C denoted the decomposition of C-H and calcium carbonate, respectively. Notably, the use of TCS reduced the contents of calcium hydroxide and calcium carbonate in cementitious materials, which is attributed to the reduction in hydration products caused by partial replacement of cement with TCS.

A similar conclusion can be obtained from the XRD results as presented in Fig. 9(b). As can be seen, the typical hydration products of cement remained unchanged with the incorporation of various CS types, including crystalline phases of C-H, ettringite (AFt), and residual C_3S and C_2S phases. Unfortunately, the main hydration product C-S-H is hard to identify in the XRD patterns due to its low crystallinity. With the application of TCS and TCS-F, the diffraction peaks of C-H crystals (about 18.0° and 34.1°) gradually weaken. The metakaolin in TCS undergoes a pozzolanic reactions in which reactive SiO_2 and Al_2O_3 react with C-H to form C-(A)-S-H [42]. Thus, it can be inferred that foam concrete with TCS has extra C-(A)-S-H gel, especially when smaller-sized TCS-F are used, which is consistent with the aforementioned TG results.

3.2.2. Microstructures

Fig. 10 shows the SEM images of various foam concrete specimens under 20 % substitution rate at 28-days. As observed in Fig. 10(a), for Sample Ref., there was remarkable inhomogeneity in pore size and a high number of connected pores, thin pore walls, and microcracks. As shown in Fig. 10(b), In the specimen using UCS, large-sized pores, most of which were interconnected and irregular, could be observed, indicating that bubbles may coalescence during the fresh-mixed state. The presence of these pores with large diameter and interconnectivity is a key factor affecting the mechanical and transport properties of foam concrete [43]. From Fig. 10(c), it can be found that the pores in the specimens containing TCS were smaller and more rounded as compared to reference specimen, although some connected pores and irregular pores were still present. In contrast, the pores in the specimen using TCS-F appeared to be much finer, highly rounded and uniformly distributed, with few interconnected and irregular pores, and with thick and dense pore walls (see Fig. 10(d)). Fig. 10(e) presents the EDS point-scan results of the typical hydration products in foam concrete using TCS. It can be found that the obvious peaks of Ca, Al and S were detected at Points 1, confirming the presence of ettringite. For Point 2, the Ca content increased while the Al content decreased, indicating that this may be a C-A-(S)-H gel. Consistent with the above chemical composition results, the metakaolin in TCS promoted cement hydration, where partial calcium hydroxide was consumed via pozzolanic reactions to form products such as C-(A)-S-H and ettringite [44], which was particularly remarkable for fine-particle metakaolin. This reduced the porosity and average pore diameter of foam concrete, forming a denser microstructure and enhancing the mechanical properties of the material [45].

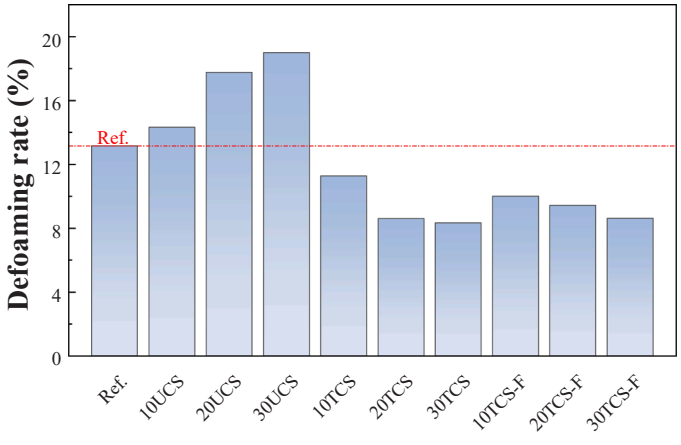

Fig. 8. Defoaming rate of fresh foam concrete.

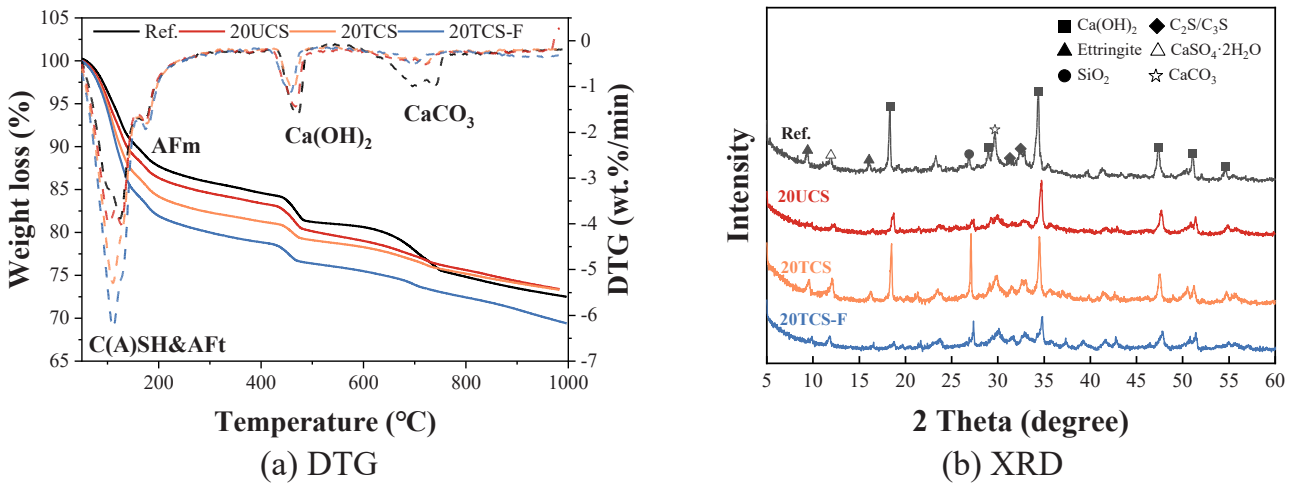

Fig. 9. DTG and XRD results of hardened foam concrete with typical mixtures.

The pore distributions of foam concrete is a critical determinant of its structural strength and transport properties. As depicted in Fig. 11, the pore size distribution varied significantly with different CS types and content. Overall, most pore sizes were concentrated in the range of 0–200 μm, while pores exceeding 400 μm were rare. The distinct pore size distributions were closely associated with the variation of the mean pore diameter. Fig. 12 presents the results of average pore size for foam concrete with different CS types and content. As the UCS content increased, the average pore size of foam concrete increased. The foam concrete with TCS or TCS-F exhibited a significantly smaller average pore size than that of samples using UCS.

Fig. 13 shows the distribution of pore roundness for foam concrete with varying mixtures. Additionally, the mean values of average pore roundness for each foam concrete specimen are plotted in Fig. 12. As the UCS admixture increased, the proportion of pores with roundness 0.9–1 decreased, while the proportion of pores with roundness 0–0.8 increased, leading to a reduction in average roundness. Furthermore, at higher replacement ratio, the proportion of pores with roundness 0.9–1 in foam concrete using TCS increased, and the overall average roundness raised, especially for specimens using TCS-F. This indicates that compared with UCS, the addition of TCS was more conducive to maintaining regular round pores in foam concrete, and the utilization of smaller particle size TCS-F further optimized the pore structure.

3.2.3. *Compressive strength*

Fig. 14 illustrates the variation of the compressive strength of foam concrete with respect to the CS replacement ratio for the 7d, 28d, and 28d water-saturated states. The trends of strength variation under different ages and conditions were similar. Taking the 28d strength as an example, the incorporation of UCS resulted in a decline, whereas the addition of TCS and TCS-F enhanced it, especially TCS-F. For instance, with the replacement ratio increased from 10 % to 30 %, the compressive strength of foam concrete using UCS decreased by about 6.1 %, 18.2 % and 26.7 % compared to Specimen Ref., while that of specimens with TCS increased by about 9.3 %, 24.3 % and 1.1 %. The study conducted by Li et al. [46] also confirmed that increasing the content of untreated CS significantly weakened the mechanical properties of foam concrete. Meanwhile, the foam concrete containing TCS-F had more significant strength gains, which were about 33.2 %, 47 %, and 48.8 % respectively

The 7d to 28d strength ratio is crucial for evaluating the strength development of foam concrete. As shown in Fig. 14, with the increase of the replacement ratio of CS, the 7d to 28d strength ratios of Groups UCS and TCS had decreasing and increasing trends, respectively. Furthermore, there was limited change in the 7d to 28d strength ratios among the TCS-F group (about 0.65), except for a significant decrease at 30 % replacement (about 0.56). It is noteworthy that the 7d strength of foam concrete was significantly reduced and the 28d strength was improved for the specimens with 30 % TCS-F as compared to specimens with low content of TCS-F.

The softening coefficient was defined as the ratio of compressive strength under 28d water-saturated state to that under 28d dried state, reflecting the ability of foam concrete to maintain strength in water and evaluating its water resistance. As shown in Fig. 14, the softening coefficient of foam concrete gradually decreased with the increase of UCS content. After thermal treatment, the softening coefficient of the material gradually increased with the increase of TCS content and the decrease of particle size (i.e., TCS-F). This phenomenon is consistent with the findings of Zhou et al. [47], who found that the foam concrete with calcined clay had excellent mechanical properties.

Fig. 15 further illustrates the relationship between the replacement ratio of CS and compressive strength of foam concrete. When using untreated UCS, the compressive strength of foam concrete had a nearly linear decrease with the replacement ratios of UCS. In contrast, after incorporating thermal-treated TCS and TCS-F, the relationship followed a binomial pattern, with a maximum value occurring at about 20 % content. Fig. 15 also presents the specific fitting formulas.

3.2.4. *Drying shrinkage behavior*

Fig. 16 shows the time-varying behavior of dry shrinkage and moisture loss in foam concrete with different CS types and content. Notably, all foam concrete groups exhibited similar shrinkage development, i.e., early-stage shrinkage strain increased rapidly, while the growth rate diminished over time. As shown in Fig. 16 (a), the drying shrinkage of foam concrete increased markedly with UCS content, whereas moisture loss decreased slightly at low UCS content but raised significantly at 30 % content. This phenomenon is consistent with the findings of Wu et al. [48], who found that the increasing untreated CS content from 25 % to 100 % raised maximum dry shrinkage by 4.5 %–38 %, and attributed to the accelerated water loss in CS-incorporated specimens. As illustrated in Fig. 16 (b-c), the drying shrinkage of foam concrete decreased with the increase in TCS and TCS-F contents. Specifically, the 28d maximum dry shrinkage strains of 10TCS, 20TCS, and 30TCS specimens were reduced by about 6.9 %, 21.2 %, and 25.5 % compared to the Specimen Ref., while the reductions for the TCS-F group were about 9.2 %, 15.9 %, and 21.6 %, respectively. This trend is similar with the experimental results of Ma et al. [30], who found that the maximum drying shrinkage rate of paste with CS decreased by 11.6 % with 30 % heat-treated CS.

In Fig. 16, the relationship between 28d relative drying shrinkage,

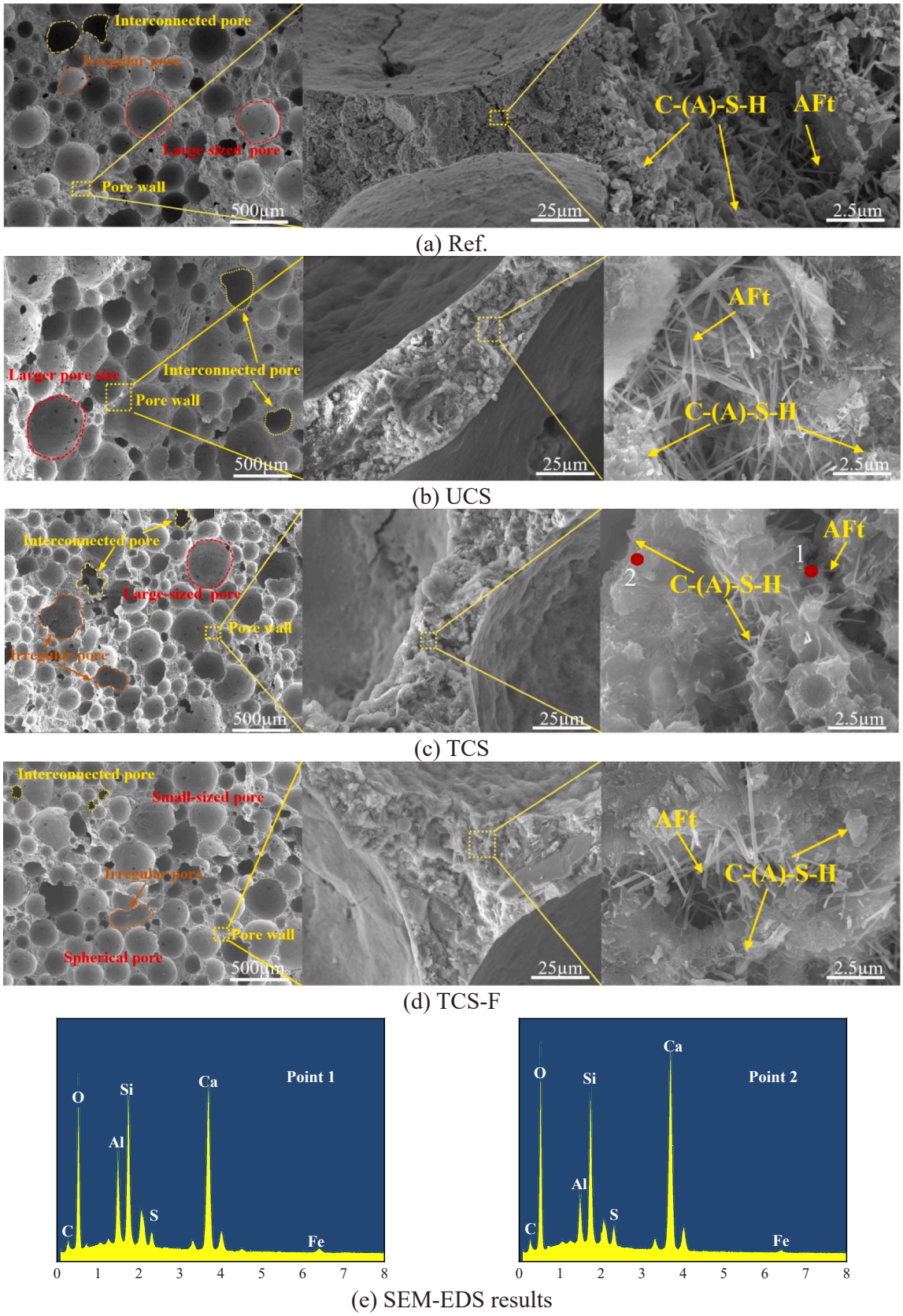

Fig. 10. Microscopic morphologies of foam concrete with varying mixtures under SEM.

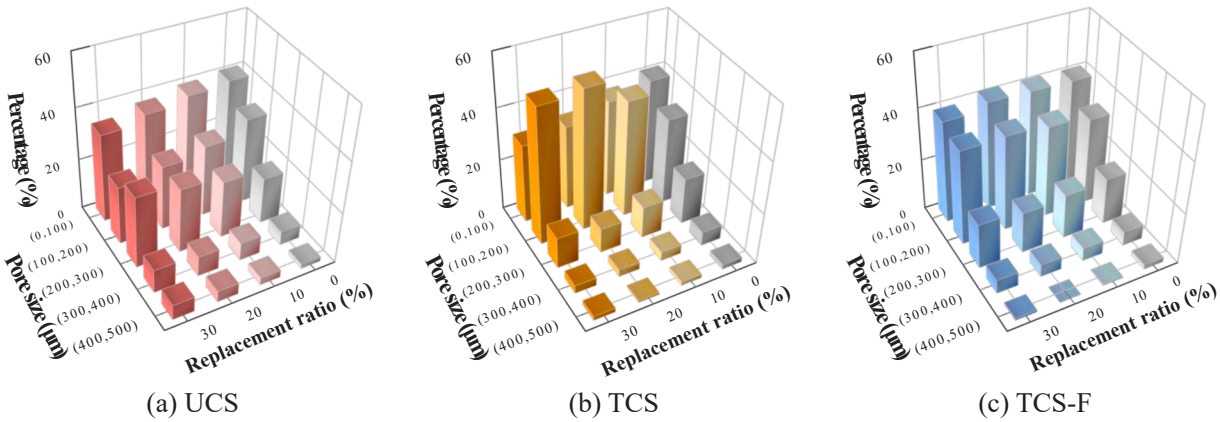

Fig. 11. Pore size distribution of foam concrete with varying mixtures.

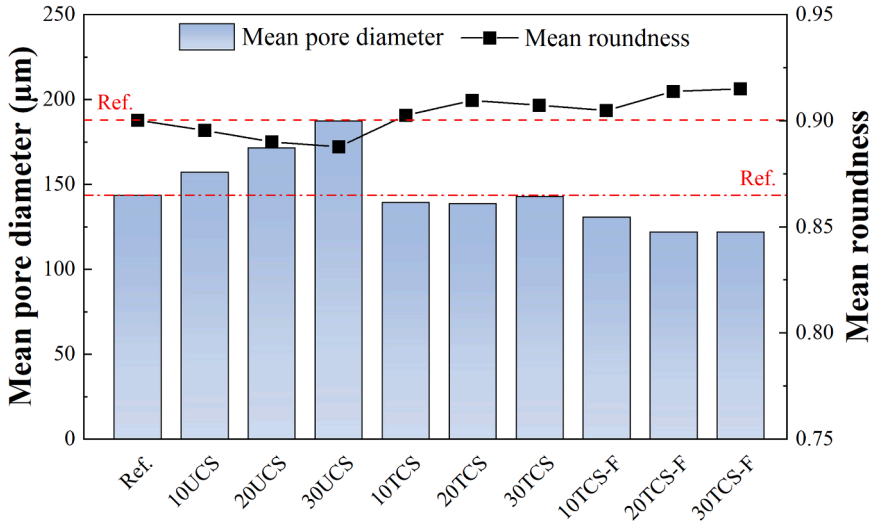

Fig. 12. Mean pore diameter and roundness of foam concrete with varying mixtures.

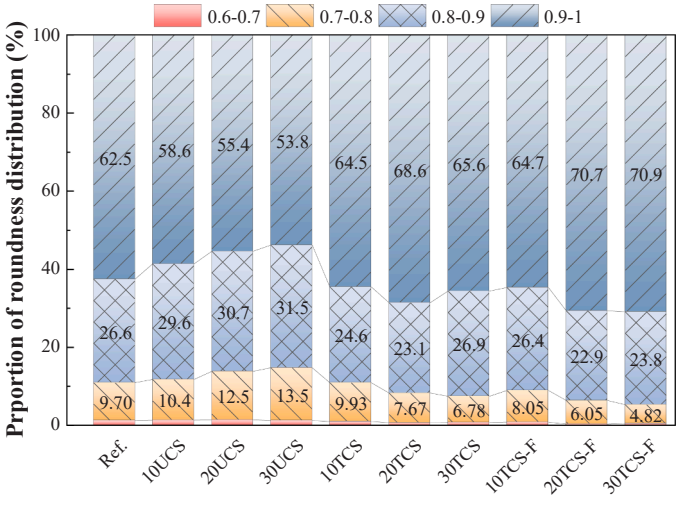

Fig. 13. Roundness distribution of foam concrete with varying mixtures.

moisture loss, and the replacement ratio of CS for foam concrete, as well as corresponding fitting formulas. The relative values were defined as the ratio of the test results of specimens with CS and that of specimens without CS. As can be seen, the relative drying shrinkage of specimens containing TCS and TCS-F had a negative linear relationship with the replacement ratio of CS. While the relative moisture loss of specimens using TCS was found to be less affected by the replacement ratio of CS, and that of specimens adding TCS-F had a negative linear correlation with the ratio.

3.2.5. *Water transport*

In this study, the capillary water absorption test was employed to characterize the water transport properties of foam concrete. Fig. 17 shows the variations in water transport properties of foam concrete with different replacement ratio of CS. It can be seen that with the increase of water absorption time, the water absorption rate of foam concrete with CS increased while the adsorption coefficient decreased, and this trend was more pronounced during the early stage of water absorption. This phenomenon may be due to the fact that the capillary pores in the material are gradually saturated with the water absorption time increases. As presented in Fig. 17, the water absorption and adsorption coefficient of foam concrete had an upward trend with increasing replacement ratios of UCS at constant absorption times. Compared to the Specimen Ref., the maximum water absorption of samples with 10 %, 20 % and 30 % UCS was enhanced by about 6.2 %, 10.8 %, and 22.1 %, respectively. This is consistent with the experimental results of Wu et al. [17], who found that increasing the content of untreated CS from 10 % to 30 % resulted in a 4.5 %–48.2 % increase in the maximum water absorption of concrete, and attributed it to the enlarged pore size and

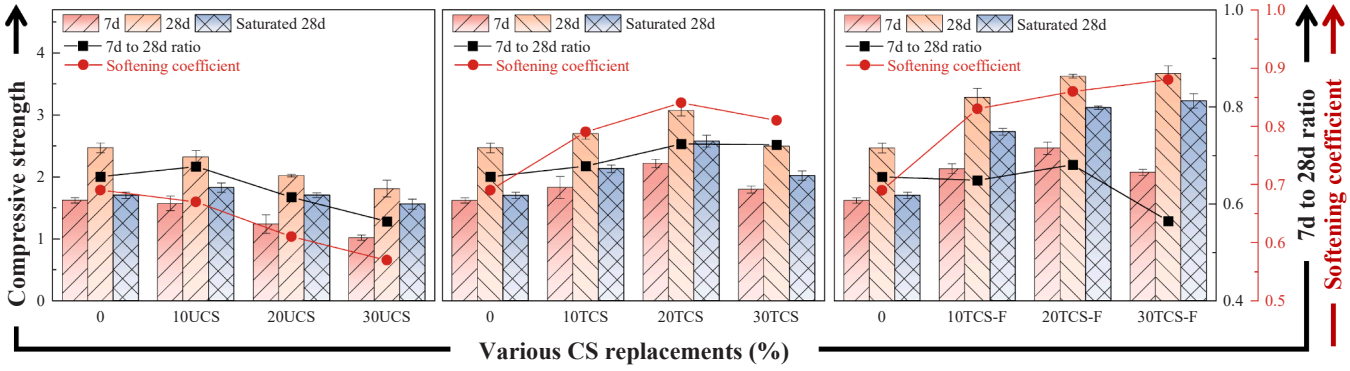

Fig. 14. Compressive strengths of foam concrete with various CS replacements.

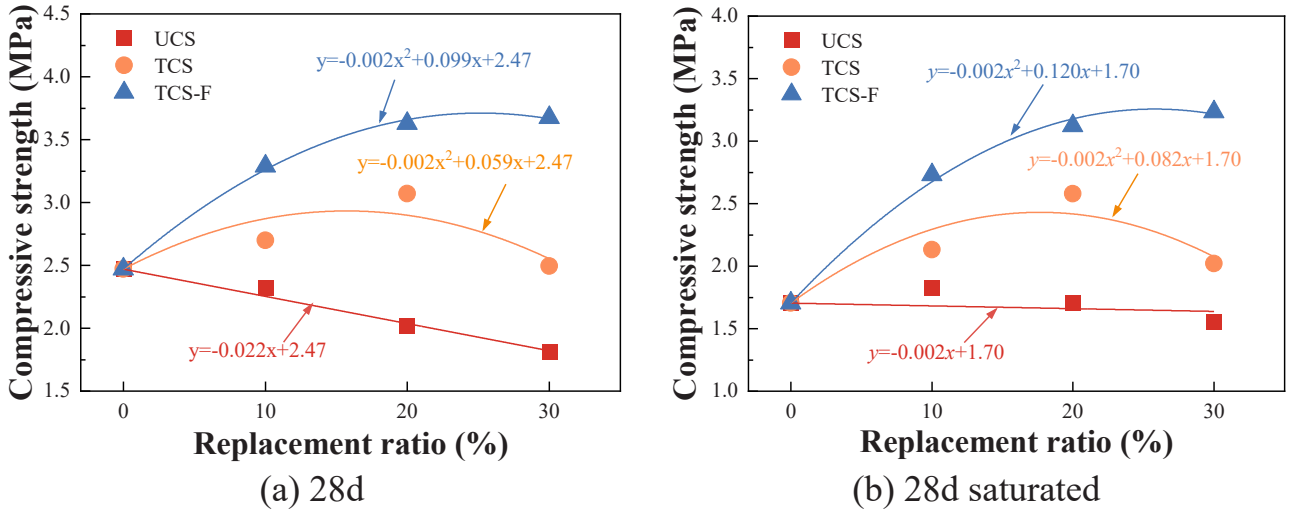

Fig. 15. Relationships between compressive strength and replacement ratios of foam concrete.

accelerated water intrusion. With the replacement ratio of TCS and TCS-F increasing from 10 % to 30 %, the water absorption and sorptivity coefficient of foam concrete at the same water absorption time were observed to first significantly increase and then stabilize.

Fig. 18 presents the relationship between porosity water absorption and drying shrinkage at different replacement ratio of CS, accompanied by mathematical expressions. It can be observed that with the increase in UCS substitution rate, the porosity and water absorption of foam concrete exhibited a linear increasing trend. When the TCS substitution rate increased, the porosity and water absorption of the material had a decreasing trend except for a slight increase at 30 % substitution. The porosity and water absorption of foam concrete were found to decrease linearly with the increase in the replacement ratio of TCS. Furthermore, the slope of linear fitting for foam concrete containing TCS-F was larger than that for foam concrete using TCS, which indicates that the use of fine-grained TCS-F more prominently enhanced the resistance to water transport in foam concrete. Fig. 18 (c) presented the relationship between total porosity and drying shrinkage as well as absorbed water amount. It can be observed that both drying shrinkage and absorbed water amount showed a positive correlation with total porosity. This can be attributed to the fact that the larger the total porosity of foam concrete, the higher the proportion of interconnected pores or large-diameter pores inside it tended to be. For the absorbed water amount, more pore spaces provide carriers for water transport. While for the drying shrinkage, the evaporation of water in the pores can cause a more obvious volume deformation.

3.3. *Sustainability evaluations*

3.3.1. *Carbon footprint*

The carbon footprint of foam concrete using CS in this study was quantified by using life cycle assessment (LCA) method which was based on the "Cradle to Gate" boundary [49]. The system boundary was mainly categorized into three stages, such as raw material production, raw material transportation, and foam concrete preparation. As per the life cycle inventory (LCI) data in relevant literatures, the CO_2 emissions in the raw material production stage are listed in Table 4. The transportation distance of various raw materials can be found in Table 4. The energy consumption of each machine in the treatment process was evaluated based on the actual working conditions in the laboratory. It is worth noting that since UCS loosed about 10 % of its bound water after thermal treatment [50], this study assumed that 1 kg of UCS produced 0.9 kg of TCS after thermally activation. From the results of particle size analysis, it was found that only 87 % of TCS could pass through a 0.15 mm sieve to become TCS-F. As per the material treatment process and carbon emission parameters of each process, the carbon emission factors of UCS, TCS, and TCS-F were calculated respectively. For the raw material transportation stage, the transportation distance from the calcination factory to the construction site was approximately 50 km [51]. Given that TCS and TCS-F need first be transported from the construction site to the thermal activation plant and then returned to the site, the transport distance was set at 100 km. The carbon emissions of each material after calculation were listed in Table 4. The carbon emission factor of cement was 0.835 kg CO_2 eq/kg, while those of TCS

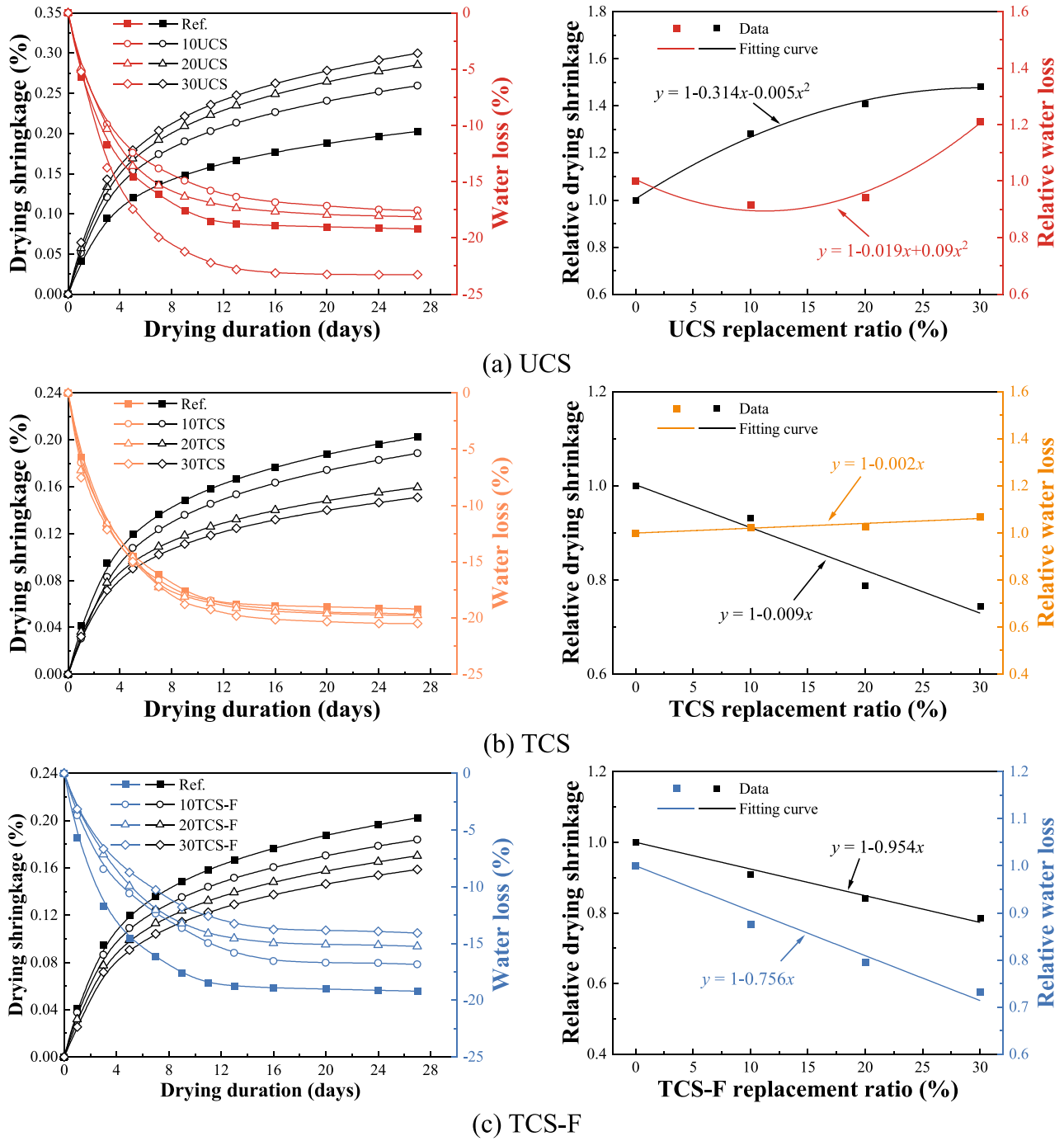

Fig. 16. Drying shrinkage behaviors of foam concrete with varying mixtures.

and TCS-F were 0.216 kg CO_2 eq/kg and 0.267 kg CO_2 eq/kg respectively, which were much lower than that of cement. This is primarily because, unlike cement clinker which requires calcination at 1300–1500°C, TCS and TCS-F only require a calcination temperature of 800°C, rendering them relatively low in carbon content.

A process-based approach was employed to analyze the carbon emissions of foam concrete in this study [52]. As per the procedures divided in Table 4, the carbon emissions for different foam concrete production were calculated by multiplying the energy consumption (M_{ik}) and carbon emission factors (Cef_k) of different stages, as shown in Eq. (10). To further compare the carbon emissions of foam concrete with different strengths, carbon emission per unit strength (i.e., CO_2 intensity) was adopted for characterization, and its calculation formula is presented in Eq. (11).

$$Carbon\ emission_i = \sum_{k=1}^{n} M_{ik} Cef_k \tag{10}$$

$$CO_2\ intensity = Carbonemission / f_{cu} \tag{11}$$

Fig. 19 illustrates the variations of carbon emissions and CO_2 intensity during the production of foam concrete using different CS. It can be observed that the carbon emissions of foam concrete decreased with the increase of CS replacement ratio. Compared with the reference specimen, the carbon emissions of specimens incorporating 10 %, 20 %, and 30 % UCS were reduced by about 9.4 %, 18.8 %, and 28.2 %, respectively. While their CO_2 intensity was slightly higher than that of the reference specimen due to the decrease in strength. As the

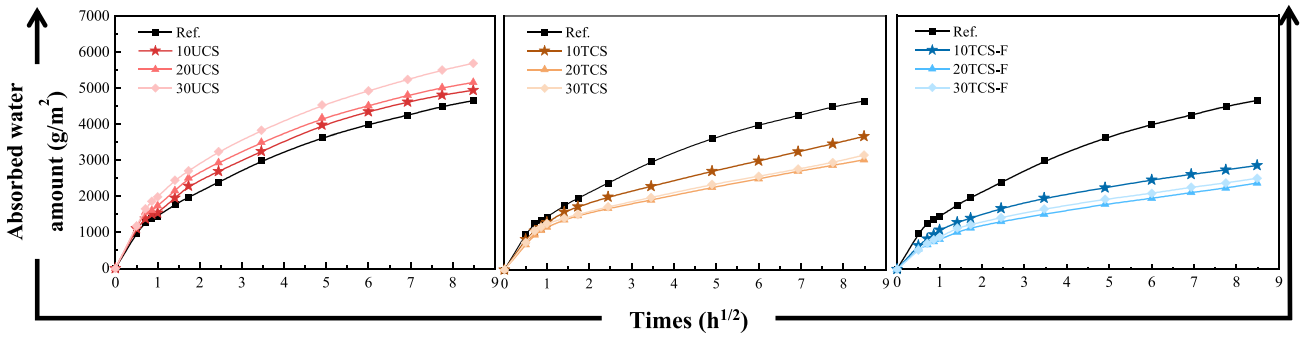

(a) Absorbed water amount

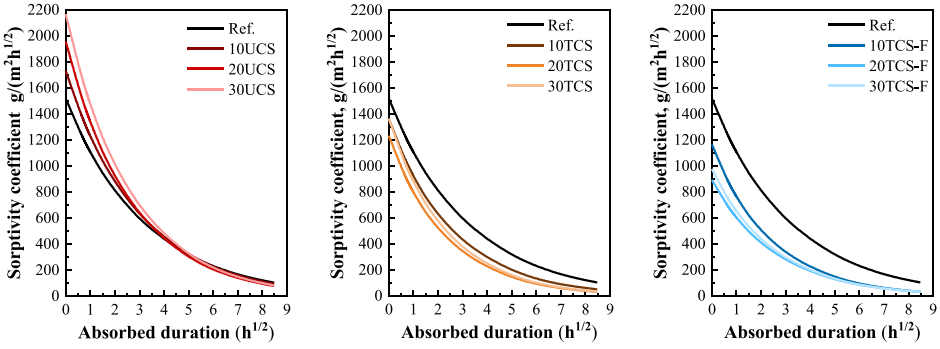

(b) Time-varying sorptivity coefficient

Fig. 17. Water absorption behaviors of foam concrete with various CS replacements.

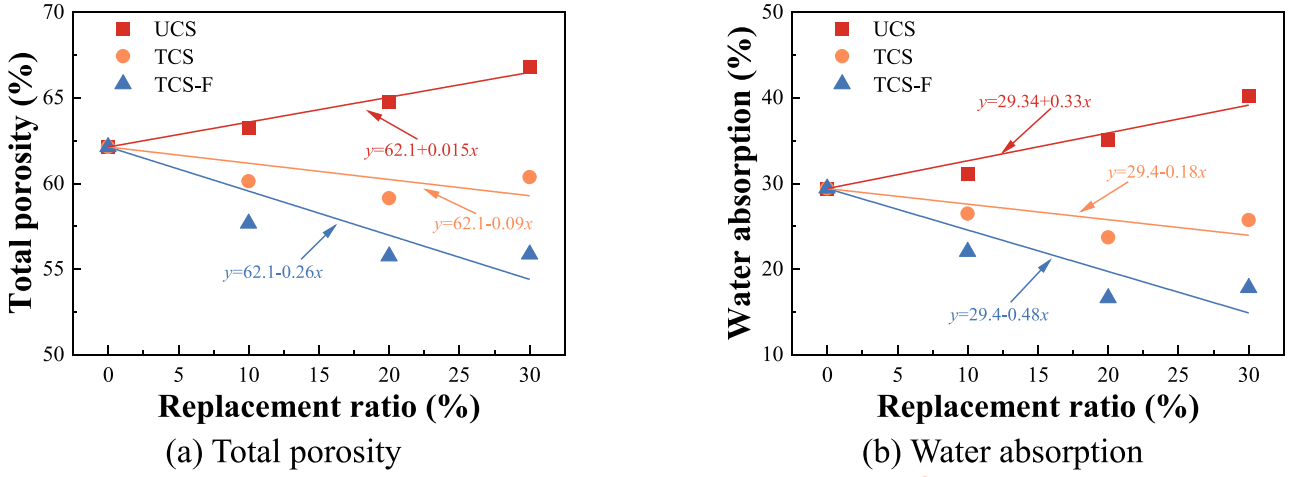

(a) Total porosity (b) Water absorption

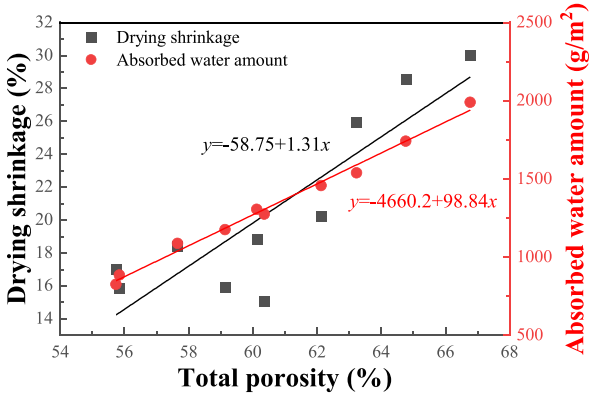

(c) The relationship between water absorption, drying shrinkage and porosity

Fig. 18. Relationship between porosity, drying shrinkage and water absorption of foam concrete with various CS replacements.

Table 4
Carbon emission factors used in this work.

Process	Sources	Machine efficiency	Cef_k	References	Transportation distance
Raw materials	Cement		0.835 kg CO_2 eq/kg	[53]	50 km
	UCS		0.02 kg CO_2 eq/kg	Calculated	0 km
	TCS		0.216 kg CO_2 eq/kg		100 km
	TCS-F		0.267 kg CO_2 eq/kg		100 km
	Water		0.0003 kg CO_2 eq/kg	[54]	0 km
	Foam		0.274 kg CO_2 eq/kg	[55]	0 km
Processing	Jaw crusher	0.005 kWh/kg	0.570 kg CO_2 eq/kWh	[51]	
	Shaker screen machine	0.03 kWh/kg			
	Ball grinding mill	0.045 kWh/kg			
	Retrofitted calciner	0.25 kWh/kg			
	Mixer	0.015 kWh/kg			
Transportation	Heavy diesel carrier car		0.129 kg CO_2 eq./(t·km)	[51]	

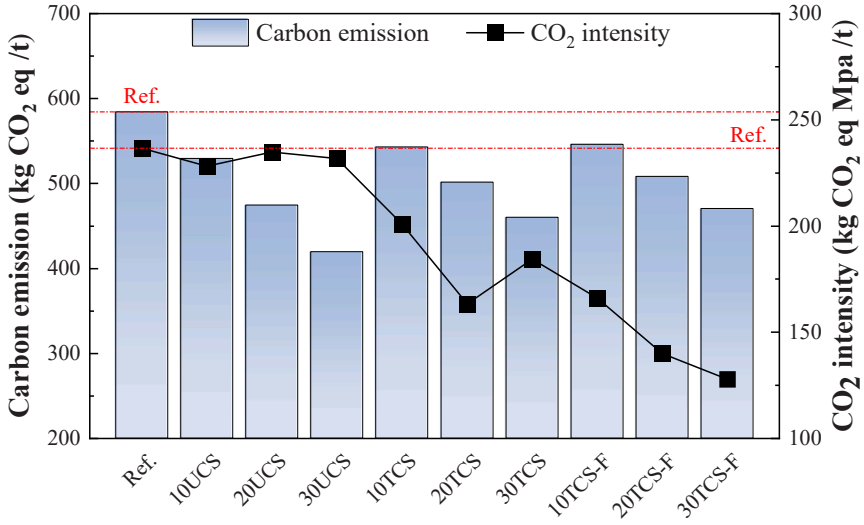

Fig. 19. LCA evaluation results of foam concrete with varying mixtures.

substitution ratio of TCS and TCS-F increased from 10 % to 30 %, the carbon emissions of the mixtures decreased by about 7.1 %-21.3 % and 6.5 %-19.5 %, respectively. The CO_2 intensity of foam concrete containing TCS showed a pattern of first decreasing and then increasing, because the decrease in strength exceeded the benefit of reduced carbon emissions when the dosage of TCS was increased to 30 %. It can be seen that with the increase of TCS-F dosage, the CO_2 intensity of the material continuously decreased by about 29.8 %-45.9 %. This is due to the fact that the addition of TCS-F improves the compressive strength of foam concrete while reducing carbon emissions.

3.3.2. Cost analysis

As per the price information for materials, industrial electricity, and transportation in Table 5. The quantification of economic costs for foam concrete was primarily based on market prices, requiring systematic research and data collection on various costs in the three stages. The cement unit price of 0.07 $/kg pegged to the US dollar was considered in the calculation of unit costs [56], which was equivalent to about 0.503 ¥/kg. The costs of UCS, TCS and TCS-F were comprehensive production costs calculated as per the energy consumption in actual technological processes (see Section 3.3.1). Regarding the initial investment for the thermal activation equipment, it is noted that this equipment can be sourced from existing cement calcination facilities without necessitating additional procurement. Consequently, this aspect has not been considered within this study.

Table 5
Unit material costs considered in the cost analysis.

Process	Cost Sources	Price	Reference
Raw materials	Cement	0.503 ¥/kg	[56]
	UCS	0.021 ¥/kg	Calculated
	TCS	0.245 ¥/kg	
	TCS-F	0.299 ¥/kg	
	Foam	0.015 ¥/kg	
	Water	0.005 ¥/kg	Investigation
Processing	Industrial electricity	0.6 ¥/kWh	Investigation
	Stirring (8 min)	0.15 ¥/t	Calculated
Transportation	Truck transport	0.5 ¥/t km	Investigation

Fig. 20 presents the costs of foam concrete with different mix proportions. It can be observed that the Ref. group had the highest cost, which was used as the benchmark for cost analysis of foam concrete. As the UCS substitution ratio increased from 10 % to 30 %, the cost of foam concrete gradually decreased. The costs of the TCS groups were lower than the Ref. group but higher than the UCS groups with the same ratio, indicating that thermally treated CS still had cost optimization potential in the preparation of foam concrete. The cost of foam concrete using TCS-F decreased with the increase of its substitution ratio, but it was always higher than that of the corresponding TCS group with the same substitution ratio. Even so, the TCS-F group still had a cost advantage over the Ref. group, e.g., a 10.5 % cost reduction for Specimen 30TCS-F.

3.3.3. Comprehensive evaluation

To consider the impact of CS and its treatment on the various properties and benefits of foam concrete, a comprehensive evaluation was carried out using an internally normalized multi-criteria analysis [57,58]. The internal normalization results for shrinkage behavior (maximum 28d shrinkage strain), moisture transfer (capillary

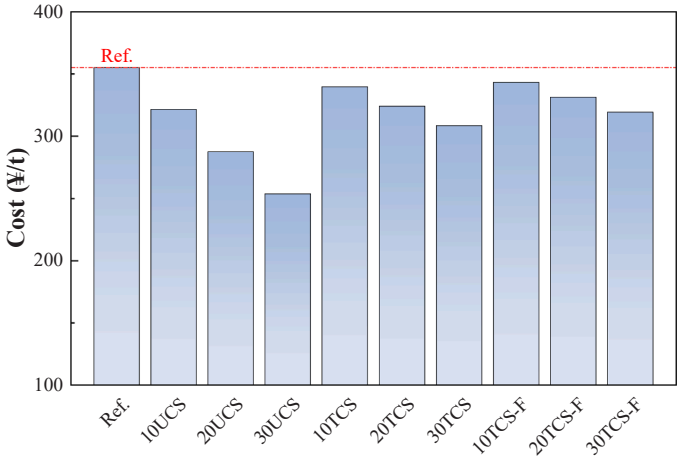

Fig. 20. Costs of foam concrete with varying mixtures.

absorption coefficient), carbon footprint and economic cost were calculated using Eq. (12). While for mechanical properties (28d compressive strength), it was determined by Eq. (13). These equations ensured that all the internally normalized results S_i^{Int} fall within the range of 0–1, where a higher score corresponds to superior performance of the corresponding indicator.

$$S_i^{Int} = \frac{\mathrm{Min}_i(r_i)}{r_i} \tag{12}$$

$$S_i^{Int} = \frac{r_i}{\mathrm{Max}_i(r_i)} \tag{13}$$

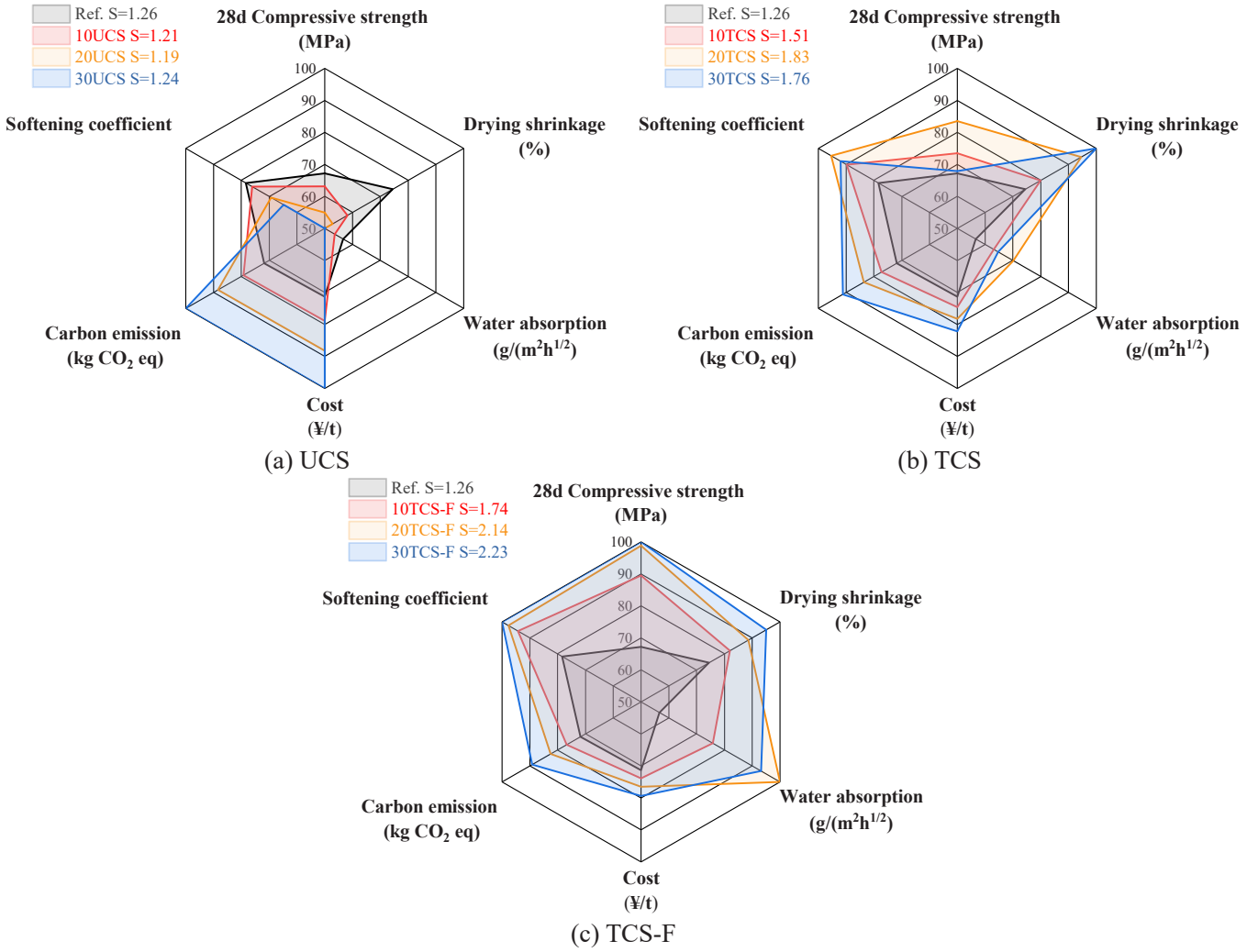

Fig. 21. Comprehensive evaluation of foam concrete with varying mixtures.

where r_i is the specific value of the corresponding performance index.

The internal normalization results of foam concrete with different types of CS were presented in the form of a radar chart, as shown in Fig. 21. A larger covered area indicates that the foam concrete with this proportion demonstrates superior comprehensive performance. Compared with the area of Specimen Ref., that of Specimens 10UCS, 20UCS and 30UCS were slightly reduced by 4 %, 5.6 % and 1.6 % respectively. The areas of Specimens 10TCS, 20TCS, and 30TCS increased by about 19.8 %, 45.2 %, and 39.7 %, respectively. When the fine-grained TCS-F was further used, the areas of the specimens at each dosage significantly increased by about 38.1 %, 69.8 % and 77 %, respectively.

It can be observed that the foam concrete with 30 % TCS-F had the largest area, demonstrating its relative superiority in comprehensive performance. Nevertheless, this does not mean that this proportion is the most recommended. For general practical application scenarios, the materials prepared with this proportion may exhibit excess performance. Moreover, its preparation process is relatively complex, involving additional thermal activation treatment and screening procedures, which leads to extra equipment and cost consumption in actual production. Additionally, some of the thermal activated coarse-grained construction waste has not been effectively utilized. However, in application scenarios where the performance of the foam concrete is critical, such as the construction of large transportation infrastructures in extreme environments, high contents of TCS-F can be added to the foam concrete preparation process. Based on the experimental and analytical results of this study, it is recommended to use a low dosage of UCS, such as 10–20 %, when thermal equipment is lacking or corresponding cost is too high. When the heat treatment conditions are met, a higher dosage of TCS, such as 20–30 %, can be used to improve its durability and service life. Given that different application scenarios impose varying performance requirements on materials, more comprehensive testing is required to investigate the relationship between the CS dosage and performance thresholds, which will further promote the practical application of CS.

4. Discussions

By combining the measured microstructures and macro-properties, Fig. 22 illustrates the potential mechanism of foam concrete containing different types of CS from fresh state to hardened state. The fluidity of fresh slurry is closely related to the pore structures of hardened foam concrete, which is controlled by the spatial distribution of free water between solid particles, the thickness of the particle surface water film, and particle morphology [59]. The use of UCS reduces the fluidity and increases yield stress and plastic viscosity of fresh slurry due to its porous structure and rough surface, while the addition of TCS improves it by reducing the internal porosity of CS particles (see Fig. 4). Furthermore, the incorporation of TCS with finer particles (i.e., TCS-F) produces a more pronounced inhibition on initial fluidity, since the decrease in particle size increases the specific surface area and inter-particle friction [60]. The time-dependent decline in slurry flowability may be attributed to more water loss over time, including water physically adsorbed by the porous particles and water consumed by the accelerated hydration reactions, which explains why increasing the TCS dosage or decreasing its particle size enhances this decline (see Fig. 5).

Although the addition of UCS increases the slurry viscosity and reduces the surface tension of fresh foam concrete (see Fig. 6), the reduction of its hydration products weakens the ability to encapsulate bubbles, and the decreased yield stress in foam gaps promotes bubble coalescence, resulting in the formation of large and unstable bubbles [61]. Under external stress, these irregular bubbles are subjected to greater pressure differentials, increasing the risk of rupture [62]. In contrast, the incorporation of TCS-F forms a uniform slurry coating around the bubbles, enhancing the yield stress of the foam gap and improving the stability of bubble distribution. This microstructural optimization prevents bubble coalescence and overlap, thereby avoiding the formation of connected pores after hardening.

Besides, the setting time of foam concrete is prolonged with increasing UCS content (see Fig. 7), which is associated with its lower reactivity compared to cement. In contrast, the use of TCS accelerates setting due to its enhanced reactivity, and the incorporation of finer TCS-F further shorten the setting time, confirming the role of particle fineness in promoting cement hydration. Generally, the earlier setting of the fresh foam concrete is favorable for improving foam stability and forming a better pore structure [63] Therefore, the foam stability in the fresh state determines the pore characteristics of the material in the hardened state.

Obviously, the pore structure significantly impacts various properties of foam concrete. Previous studies have shown that the sphericity of pores enhances stress distribution and material strength [64]. The incorporation of UCS tends to form oversized and irregularly shaped interconnected pores (see Fig. 10), which significantly compromises the geometric regularity of the pore structure and creates stress concentration points that reduce the strength of material. Furthermore, this interconnected pore network facilitates moisture, and exacerbate drying shrinkage phenomena. In contrast, the use of thermal-activated TCS and fine-grained TCS-F is effective in improving the pore structure of foam

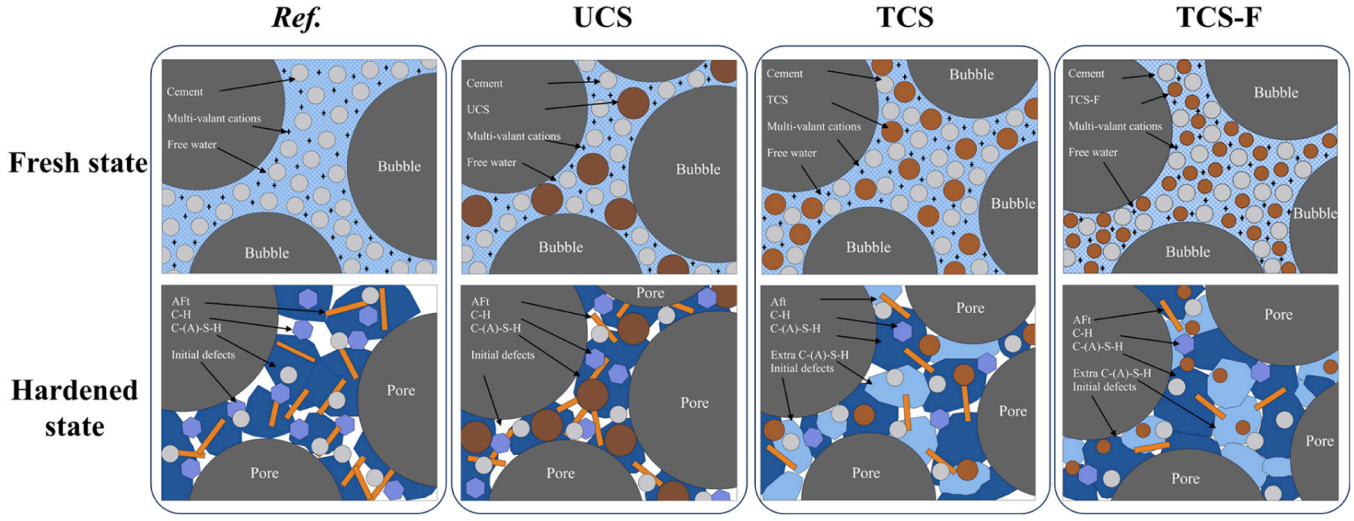

Fig. 22. Schematic diagram of foam concrete with different CS types.

concrete. Specimens incorporating these materials have a reduction in average pore size and an increase in pore sphericity. More significantly, the reactive components (mainly metakaolin) in TCS undergo pozzolanic reactions to produce hydration products including C-(A)-S-H gel and ettringite, which effectively fill initial defects and improve the compactness of pore walls (see Fig. 10). The optimization of these microstructures improves the mechanical properties of the material, reduces the water loss and drying shrinkage, results in more tortuous transport pathways for water. While as the TCS content is increased to 30 %, the pore structure begins to deteriorate and the strength exhibits a decreasing trend, which might be attributed to the dilution effect of high replacement [65] and the insufficient C-H supply for pozzolanic reactions [66].

5. Conclusions

This study systematically investigates the effects of construction spoil (CS) with different types, contents, and particle sizes as a cement substitute on the microstructures and macroscopic properties of foam concrete. The main research findings are summarized as follows:

1. The incorporation of UCS reduced the fluidity and increased yield stress and plastic viscosity of fresh mixture due to its high water-absorption and low activity, prolonged the setting time, and increased the defoaming rate by about 8.8 %-44.5 %. The use of thermally activated TCS and TCS-F resulted in a smaller decrease in material workability, shortened the setting time, formed an early-stage stable skeleton, and decreased the defoaming rate by about 14.4 %-36.7 %, improving the foam stability of foam concrete.
2. The use of UCS significantly reduced the number of hydration products in foam concrete, increased the pore size and the number of connected and irregular pores, which led to a decrease of compressive strength and softening coefficient, as well as an increase of drying shrinkage and water absorption.
3. The addition of thermal-activated CS resulted in the formation of denser pore wall, smaller and rounder pores due to the pozzolanic reaction and filling effect produced by the generated metakaolin. As the particle size of thermoactivated CS decreased, the number of small-sized and spherical pores was further increased. The incorporation of TCS and TCS-F could improve the strength, water stability and water absorption of foam concrete using CS, as well as reduced the water loss and shrinkage under dry conditions.
4. Using untreated and thermal-activated CS could both reduce the carbon emissions and costs of foam concrete, and the reduction was larger in the case of the former, up to about 28.2 % and 13.2 %, respectively. While the use of thermoactivated CS had a more significant effect in reducing the CO_2 intensity.

CRediT authorship contribution statement

Junhui Zhang: Writing – review & editing, Supervision, Project administration, Funding acquisition, Conceptualization. **Yu Wang:** Writing – original draft, Investigation, Formal analysis, Data curation. **Yuxiang Tang:** Writing – review & editing, Methodology, Funding acquisition, Conceptualization. **Xufu Wang:** Writing – review & editing, Investigation. **Fan Gu:** Writing – review & editing. **Jianzhuang Xiao:** Writing – review & editing. **Li jianxing:** Writing – review & editing. **Mingzhong Zhang:** Writing – review & editing.

Declaration of Competing Interest

The authors declare that they have no known competing financial interests or personal relationships that could have appeared to influence the work reported in this paper.

Acknowledgments

The authors acknowledge the support of the National Natural Science Foundation of China (grant number: 52361165623, 52408464, 52025085), the China Postdoctoral Science Foundation (grant number: 2025T180894, 2025M773268) and the Postdoctoral Fellowship Program of CPSF (grant number: GZB20240636), and the Science Fund for Creative Research Groups of Hunan Provincial Natural Science Foundation (grant number: 2024JJ1001).

Data availability

Data will be made available on request.

References

[1] Y. Jin, X. Wang, W. Huang, X. Li, Q. Ma, Mechanical and durability properties of hybrid natural fibre reinforced roadbed foamed concrete, Constr. Build. Mater. 409 (2023) 134008.
[2] N. Zhang, X. Guo, Y. Li, J. Zhang, T. Yu, Composition design and crack resistance optimization method of red mud based foamed lightweight soil, J. Ceram. Process. Res. 25 (3) (2024) 355–364.
[3] G. Moumin, M. Ryssel, L. Zhao, P. Markewitz, C. Sattler, M. Robinius, D. Stolten, CO2 emission reduction in the cement industry by using a solar calciner, Renew. Energy 145 (2020) 1578–1596.
[4] D. Fan, X. Lv, J. Lu, R. Yu, W. She, J. Moon, T. Noguchi, C. Poon, Ultra-stable CO2-aqueous foams for carbon sequestration and internal mineralization in cellular cements, Chem. Eng. J. 515 (2025) 163477.
[5] L. Jiang, Z. Wang, Y. Wang, J. Niu, J. Qin, Preparation and properties of carbon dioxide foamed concrete using nanoparticles as foam stabilizer and pre-carbonated cement slurry, Cem. Concr. Compos. 151 (2024) 105585.
[6] D. Fan, C. Zhang, X. Li, X. Lv, J. Lu, R. Yu, T. Noguchi, C. Poon, Development of foam concrete toward high strength and CO2 sequestration, ACS Sustain. Chem. Eng. 12 (45) (2024) 16622–16637.
[7] Y. Zhang, Y. Jiang, T. Ling, Use of CO2 as a controlled foam stabilizer to enhance pore structure and properties of foamed concrete, Cem. Concr. Compos. 145 (2024) 105356.
[8] Y. Tang, J. Xiao, H. Zhang, D. Wang, M. Zhang, J. Zhang, Effect of accelerated carbonation of fully recycled aggregates on fracture behaviour of concrete, Cem. Concr. Compos. 148 (2024) 105442.
[9] C. Chen, X. Wang, Y. Wang, S. Jiu, Y. Chen, Effect of rock-wool waste on physical, mechanical, and microscopic properties of nonburn solid bricks, Constr. Build. Mater. 392 (2023) 131805.
[10] A. Ali, Aliabdo, M. Abd-Elmoaty, Hani Abd-Elmoaty, H. Hassan, Utilization of crushed clay brick in cellular concrete production, Alex. Eng. J. 53 (1) (2014) 119–130.
[11] J. Dang, X. Tang, J. Xiao, Z. Duan, A. Han, Role of recycled brick powder and alkaline solution on the properties of eco-friendly alkali-activated foam concrete, J. Clean. Prod. 436 (2024) 140381.
[12] K. Pasupathy, S. Ramakrishnan, J. Sanjayan, Formulating eco-friendly geopolymer foam concrete by alkali-activation of ground brick waste, J. Clean. Prod. 325 (2021) 129180.
[13] J. Xiao, J. Shen, M. Bai, Q. Gao, Y. Wu, Reuse of construction spoil in China: Current status and future opportunities, J. Clean. Prod. 290 (2021) 125742.
[14] Z. Ma, J. Shen, C. Wang, H. Wu, Characterization of sustainable mortar containing high-quality recycled manufactured sand crushed from recycled coarse aggregate, Cem. Concr. Compos. 132 (2022) 104629.
[15] F. Gu, J. Xie, C. Vuye, Y. Wu, J. Zhang, Synthesis of geopolymer using alkaline activation of building-related construction and demolition wastes, J. Clean. Prod. 420 (2023) 138335.
[16] Y. Tang, J. Xiao, Q. Liu, B. Xia, A. Singh, Z. Lv, W. Song, Natural gravel-recycled aggregate concrete applied in rural highway pavement: material properties and life cycle assessment, J. Clean. Prod. 334 (2022) 130219.
[17] H. Wu, P. Yao, D. Yang, J. Shen, Z. Ma, C. Wang, Upcycling of construction spoil powder as partial cement replacement for sustainable cement-based materials: Properties and modification, J. Clean. Prod. 369 (2022) 133361.
[18] K. Geng, J. Chai, Y. Qin, Z. Xu, J. Cao, X. Zhang, Material characteristics and pollutant diffusion simulation of cutoff walls made of alkali activated slag/bentonite, Dev. Built Environ. 15 (2023) 100200.
[19] J. Shen, J. Xiao, T. Ye, S. Li, Novel formula design of alkali-activated slag solidified construction spoil considering flowability and compressive strength, J. Build. Eng. 96 (2024) 110517.
[20] J. Ren, H. Sun, Q. Li, Z. Li, L. Ling, X. Zhang, Y. Wang, F. Xing, Experimental comparisons between one-part and normal (two-part) alkali-activated slag binders, Constr. Build. Mater. 309 (2021) 125177.
[21] J. Skibsted, R. Snellings, Reactivity of supplementary cementitious materials (SCMs) in cement blends, Cem. Concr. Res. 124 (2019) 105799.
[22] L. Ling, J. Yang, W. Yao, F. Xing, H. Sun, Y. Li, Recycled excavation soils as sustainable supplementary cementitious materials: kaolinite content and performance implications, Materials 17 (10) (2024) 2289.

[23] Z. He, R. Hu, Z. Ma, X. Liu, C. Wang, H. Wu, Reusing thermoactivated construction waste spoil as sustainable binder for durable concrete: microstructure and chloride transport, Constr. Build. Mater. 398 (2023) 132553.
[24] Y. Song, D. Lange, Influence of fine inclusions on the morphology and mechanical performance of lightweight foam concrete, Cem. Concr. Compos. 124 (2021) 104264.
[25] P. Favaretto, G. Hidalgo, C. Sampaio, R. Silva, R. Lermen, Characterization and use of construction and demolition waste from South of Brazil in the production of foamed concrete blocks, Appl. Sci. 7 (10) (2017) 1090.
[26] J. Liu, H. Li, R. Wang, Y. Hou, S. Godang, Formation process of a newly explored ion-adsorption type REE deposit in Pingtian, Guangdong, South China: a detailed profile analysis, Geochemistry 85 (3) (2025) 126302.
[27] Y. Li, P. Yi, H. Du, W. Liu, T. Mi, L. Huang, X. Gao, X. Sun, F. Xing, Activation of locally excavated spoil for utilization in limestone calcined clay cement (LC3), Constr. Build. Mater. 420 (2024) 135518.
[28] GB/T 50123, 2019, Standard for geotechnical testing method, Standardization Administration of the People's Republic of China, PR China.
[29] T. Hanein, K. Thienel, F. Zunino, A. Marsh, M. Maier, B. Wang, M. Canut, M. Juenger, M. Ben Haha, F. Avet, A. Parashar, L. Al-Jaberi, R. Almenares-Reyes, A. Alujas-Diaz, K. Scrivener, S. Bernal, J. Provis, T. Sui, S. Bishnoi, F. Martirena-Hernández, Clay calcination technology: state-of-the-art review by the RILEM TC 282-CCL, Mater. Struct. 55 (1) (2022) 3.
[30] Z. Ma, Q. Tang, H. Wu, J. Xu, C. Liang, Mechanical properties and water absorption of cement composites with various fineness and contents of waste brick powder from C&D waste, Cement and Concrete, Composites 114 (2020) 103758.
[31] S. Cheng, K. Ge, T. Sun, Z. Shui, J.X. Lu, Pozzolanic activity of mechanochemically and thermally activated coal-series kaolin in cement-based materials, Constr. Build. Mater. 299 (6) (2021) 123972.
[32] M. Morsy, H. Shoukry, M. Mokhtar, A. Ali, S. El-Khodary, Facile production of nano-scale metakaolin: An investigation into its effect on compressive strength, pore structure and microstructural characteristics of mortar, Constr. Build. Mater. 172 (2018) 243–250.
[33] JGJ/T 341, 2014, Technical specification for application of foamed concrete, Ministry of Housing and Urban Rural Development of the People's Republic of China, PR China.
[34] D. Fan, C. Zhang, J. Lu, L. Peng, R. Yu, C. Poon, Rheology dependent pore structure optimization of high-performance foam concrete, Cem. Concr. Res. 188 (2025) 107737.
[35] TJG F1001, Technical specification for design and construction of cast-in-situ foamed lightweight soil subgrade, Tianjin Municipal Highway Management Bureau, PR China, 2011.
[36] JG/T 266, 2011, Foamed concrete, Ministry of Housing and Urban Rural Development of the People's Republic of China, PR China.
[37] CJJ/T 177, Technical specification for foamed mixturelightweight soil filling engineering, Ministry of Housing and Urban Rural Development of the People's Republic of China, PR China, 2012.
[38] GB/T 11969, 2020, Test methods of autoclaved aerated concrete, Standardization Administration of the People's Republic of China, PR China.
[39] Y. Chen, J. Li, J. Jin, P. Wang, L. Han, X. Chen, C. Xu, S. Fu, Y. Xu, Recycling of calcareous shield tunnel muck and industrial solid waste for preparation of self-consolidating backfill slurry: Perspectives on fluidity, mechanical properties, and carbon footprints, Case Stud. Constr. Mater. 23 (2025) e05357.
[40] O. Canbek, Q. Xu, Y. Mei, N. Washburn, K. Kurtis, Predicting the rheology of limestone calcined clay cements (LC3): linking composition and hydration kinetics to yield stress through Machine Learning, Cem. Concr. Res. 160 (2022) 106925.
[41] X. Dai, M. Yio, H. Wu, S. Lopez, C. Cheeseman, H. Wong, Enhancing the rheology, reaction kinetics and early-age strength of limestone calcined clay cement (LC3) with sodium silicate addition, Cem. Concr. Res. 198 (2025) 107997.
[42] F. Avet, K. Scrivener, Investigation of the calcined kaolinite content on the hydration of Limestone Calcined Clay Cement (LC3), Cem. Concr. Res. 107 (2018) 124–135.
[43] G. Sang, Y. Zhu, G. Yang, H. Zhang, Preparation and characterization of high porosity cement-based foam material, Constr. Build. Mater. 91 (2015) 133–137.
[44] P. Shen, L. Lu, W. Chen, F. Wang, S. Hu, Efficiency of metakaolin in steam cured high strength concrete, Constr. Build. Mater. 152 (2017) 357–366.
[45] J. Dang, X. Tang, J. Xiao, A. Han, Influence of alkaline activator and precursor on the foam characterization and alkali-activated foamed concrete properties, Cem. Concr. Compos. 145 (2024) 105341.
[46] W. Li, J. Yang, M. Sun, F. Xu, Y. Zhao, H. Xia, A sludge-modified foam concrete for road fill material: Performance evaluation and carbon footprint analysis, J. Co2 Util. 91 (2025) 103006.
[47] G. Zhou, Y. Zhu, R.K.L. Su, Novel high performance green calcined clay-based foam concrete, J. Build. Eng. 110 (2025) 113069.
[48] H. Wu, C. Wang, Z. Ma, Drying shrinkage, mechanical and transport properties of sustainable mortar with both recycled aggregate and powder from concrete waste, J. Build. Eng. 49 (2022) 104048.
[49] J. Xiao, H. Zhang, Y. Tang, Q. Deng, D. Wang, C. Poon, Fully utilizing carbonated recycled aggregates in concrete: Strength, drying shrinkage and carbon emissions analysis, J. Clean. Prod. 377 (2022) 134520.
[50] Y. Ruan, T. Jamil, C. Hu, B. Gautam, J. Yu, Microstructure and mechanical properties of sustainable cementitious materials with ultra-high substitution level of calcined clay and limestone powder, Constr. Build. Mater. 314 (2022) 125416.
[51] J. Shen, J. Xiao, G. Wen, Z. Xi, S. Li, Orthogonal test of alkali-activated slag solidified construction spoil, fluidity, compressive strength, water resistance and carbon emission, J. Clean. Prod. 434 (2024) 140201.
[52] A. Fenner, C. Kibert, J. Woo, S. Morque, M. Razkenari, H. Hakim, X. Lu, The carbon footprint of buildings: a review of methodologies and applications, Renew. Sustain. Energy Rev. 94 (2018) 1142–1152.
[53] X. Huang, Z. Jiao, F. Xing, L. Sui, B. Hu, Y. Zhou, Performance assessment of LC3 concrete structures considering life-cycle cost and environmental impacts, J. Clean. Prod. 436 (2024) 140380.
[54] X. Wei, J. Zhu, C. Pei, Tailored water-based graphene nanofluid additives for high-performance, low-carbon, and cost-effective nanoengineered concrete, Constr. Build. Mater. 483 (2025) 141788.
[55] Q. Liu, Y. Wang, C. Sun, S. Cheng, C. Yang, Carbon sequestration and mechanical properties of foam concrete based on red mud pre-carbonation and CO2 foam bubbles, Constr. Build. Mater. 426 (2024) 135961.
[56] M. Davraz, N. Isildar, A.N. Kaplan, Investigation of the effects of steam curing of concrete at different temperatures on cost and compressive strength by response surface methodology, Constr. Build. Mater. 470 (2025) 140589.
[57] X. Chen, H. Wang, H. Najm, G. Venkiteela, J. Hencken, Evaluating engineering properties and environmental impact of pervious concrete with fly ash and slag, J. Clean. Prod. 237 (2019) 117714.
[58] H. Wang, J.J. Wu, X. Zhu, Q. Liao, L. Zhao, Energy–environment–economy evaluations of commercial scale systems for blast furnace slag treatment: dry slag granulation vs. water quenching, Appl. Energy 171 (2016) 314–324.
[59] J. Chen, Q. Li, P. Ng, L. Li, A. Kwan, Cement equivalence of metakaolin for workability, cohesiveness, strength and sorptivity of concrete, Materials 13 (7) (2020) 1646.
[60] H. Jing, M. Li, Y. Zhang, M. Gao, Hydration kinetics, microstructure and physicochemical performance of metakaolin-blended cementitious composites, Constr. Build. Mater. 408 (2023) 133756.
[61] C. Liu, Z. Zhang, Z. Jia, R. Cao, W. Wang, N. Banthia, C. Chen, Y. Xiong, Y. Chen, Y. Zhang, Quantitative characterization of bubble stability of foam concrete throughout extrusion process: From yield stress, viscosity and surface tension point of view, Compos. Part BEng. 284 (2024) 111724.
[62] A. Oratis, J. Bush, H. Stone, J. Bird, A new wrinkle on liquid sheets: Turning the mechanism of viscous bubble collapse upside down, Science 369 (6504) (2020) 685. −+.
[63] K. Dhasindrakrishna, S. Ramakrishnan, K. Pasupathy, J. Sanjayan, Collapse of fresh foam concrete: Mechanisms and influencing parameters, Cem. Concr. Compos. 122 (2021) 104151.
[64] Y. Chen, Y. Zhang, Z.N. Banthia, Unraveling pore structure alternations in 3D-printed geopolymer concrete and corresponding impacts on macro-properties, Addit. Manuf. 59 (Part:A) (2022) 103137.
[65] A. Tironi, C. Castellano, V. Bonavetti, M. Trezza, A. Scian, E. Irassar, Kaolinitic calcined clays - Portland cement system: hydration and properties, Constr. Build. Mater. 64 (2014) 215–221.
[66] T. Oey, A. Kumar, J. Bullard, N. Neithalath, G. Sant, The filler effect: the influence of filler content and surface area on cementitious reaction rates, J. Am. Ceram. Soc. 96 (6) (2013) 1978–1990.